SHIRSHOV INSTITUTE OF OCEANOLOGY

CRUISE REPORT No. 77

RV *AKADEMIK MSTISLAV KELDYSH* CRUISE 07 August – 15 September 2019

North Atlantic Repeat Hydrography of the section along 59.5 N and the Denmark Strait Experiment II

Principal Scientist **S. Gladyshev**[1]

2019

Shirshov Institute of Oceanology
36 Nakhimovskii prospect
Moscow 117997 RUSSIA
Tel: +7(495) 719 0255 Fax: +7(499) 124 6342
Email :sgladyshev@ocean.ru

[1]**Shirshov Institute of Oceanology**

DOCUMENT DATA SHEET

AUTHOR GLADYSHEV, S	***PUBLICATION DATE*** 2019
TITLE RV ***Akademik Mstislav Keldysh*** Cruise 77, 07 August – 15 September 2019.	
REFERENCE Shirshov Institute of Oceanology, Akademik Mstislav Keldysh Cruise Report, No. 77, 75 p. Fig. and Tables	

ABSTRACT

RV ***Akademik Mstislav Keldysh*** Cruise 77 was a contribution to the Russian CLIVAR and State Research Programmes. CTD sections were designed to enable the ocean circulation in the Subpolar gyre of the North Atlantic to be mapped and in particular the course of the North Atlantic Current branches. The main goal is to continue annual monitoring of the North Atlantic large-scale circulation and climate changes in the North Atlantic started in 1997. The Denmark Strait Experiment II was the second part of 7-day experiment carried out in July 2018. It was designed to understand the mechanisms of short-term variability of water exchange between the North Atlantic and the Nordic Seas.

KEYWORDS

CRUISE 77 2019, *AKADEMIK MSTISLAV KELDYSH,* **CLIVAR, TRANSATLANTIC SECTION, NORTH ATLANTIC SUBPOLAR GYRE, DEEP WINTER CONVECTION, CTD OBSERVATIONS, LADCP, VMADCP, DENMARK STRAIT, WATER EXCHANGE, SHORT-TERM VARIABILITY.**

ISSUING ORGANISATION

Shirshov Institute of Oceanology
36 Nakhimovskii prospect
Moscow 117997 RUSSIA

Active Director: Dr. Alexey Sokov

Copies of this report are available from: **Marine Expedition Centre,** Tel: +7(495)7190255 Fax: +7(499)124 6342

Email: **sgladyshev@ocean.ru**

Contents

Scientific Personnel

GLADYSHEV, S.	Principal Scientist	Shirshov
POLITOVA, N.	Deputy Chief	Shirshov
GLADYSHEV, V.	Chief of CTD group	Shirshov
ZAPOTYL'KO, V.	CTD, LADCP	Shirshov
GAVRIKOV, A.	CTD, LADCP	Shirshov
VEREZEMSKAYA, P.	CTD, LADCP	Shirshov
SHARMAR, V.	CTD, Sampling	Shirshov
LUKASHIN, S.	Winch	Shirshov Atlantic Branch
MUKHAMETYANOV, R.	Sampling	MFTI
ZAMYATIN, E.	Sampling	MGU
PYATAKOV, V.	Sampling	Shirshov Atlantic Branch
KOLOKOLOVA, A.	Chief of Chemistry group	Shirshov
MELNIKOVA, Z.	Nutrients	Shirshov
MERKULOVA, M.	Nutrients	Shirshov
NETSVETAEVA, O.	Oxygen	Shirshov
DEMIDOV, A.	Chief of PP group	Shirshov
GAGARIN, V.	Primary Production, Chl A	Shirshov
MALAPHEEV, Yu.	Ghief of geological group	Shirshov Atlantic Branch
BULOKHOV, A.	Moorings, Gravity Corer	Shirshov
ISACHENKO, S.	Moorings, Gravity Corer	Shirshov Atlantic Branch
STARODYMOVA, D.	Ghief of suspended sediment group	Shirshov
MAKHNOVICH, N.	Suspended Sediment Treatment	Shirshov NW Branch
SLOMNYUK, S.	Suspended Sediment Treatment	MGRI
SANTANA, M.	Carbonate system	University of Las Palmas
GONZÁLEZ, M.	Carbonate system	University of Las Palmas
ALAMO, A.	Carbonate system	University of Las Palmas

1. CRUISE NARRATIVE

1.1 Cruise Details

Expedition Designation: R/V ***Akademik Mstislav Keldysh*** Cruise 77, RUSSIA CLIVAR

Principal Scientist: Dr. Sergey V. Gladyshev (Shirshov).

Ship: RV ***Akademik Mstislav Keldysh.***

Ports of Call: Arkhangelsk (Russia) to Arkhangelsk (Russia).

Cruise Dates: 07th August to 15th September 2019.

1.2 Cruise Summary

1.2.1 Cruise Track and Stations

The cruise track with station positions is shown in **Fig. l**. Only small volume samples were taken, details are listed in **Table 1**.

1.2.2. Equipment

The principal instruments used during the cruise were a SBE 9P-1277 and 0727 CTDs with dual temperature and conductivity sensors (SBE 3 SN 03P6082, SBE 4 SN 044580, SBE 3 SN 03P6088, SBE 4 SN 044581), oxygen sensors (SBE 43 SN 3321 and SN0699), fluorimeter-turbidity sensor (WET Labs, SN 4237), Benthos altimeter model PSD 916 SN 1069, LADCP WHS-300 kHz down-looking (S/N 6393), LADCP WHS-300 kHz up-looking (S/N 14151). These were mounted together with a multisampler Carousel SBE 32 equipped with 22 5-litre Niskin bottles. Upon recovery each bottle was sampled in turn for dissolved oxygen, nutrients, salinity, primary production, chlorophyll a, and suspended matter, DIC, PH, Alkalinity and TOC. All sampling was done on deck. Currents were measured using vessel mounted ADCP (VMADCP) TRDI OS75 kHz (S/N 671849) installed at the central point of the ship hall.

3D navigation information was provided by a Trimble SPS 855/555H - Modular GPS receiver together with MRU 3 (Kongsberg) and every second was recorded on the PC. Additional measurements were made with an EA600 12 kHz and Vaisala meteorological package.

1.2.3 Sampling

Nominal depths sampled were: bottom, 3100, 3000, 2750, 2500, 2250, 2000, 1750, 1500, 1250, 1100, 1000, 900, 800, 700, 600, 500, 400, 300, 200, 150, 100, 50, 30, 20, 10 m. On deep casts fewer shallow and intermediate bottles were fired. The actual bottle depths are shown in **Fig. 2**.

1.2.4 Number of Stations Occupied

163 stations (171 casts) were occupied during the cruise (**Fig. l**).

1.3 Scientific Objectives

The cruise objectives were to:

1. To complete a CTD section from Scotland to Greenland.
2. To carry out the Denmark Strait Experiment II.
3. To provide mooring recoveries in the North Atlantic.

1.4 Narrative

1.4.1 Introduction

The meridional overturning circulation (MOC) in the North Atlantic is one of the main drivers of the widely known global oceanic “conveyor belt” – an important element of the Earth’s climate system [e.g., van Aken, 2007]. Warm upper-ocean waters transported northward by the North Atlantic Current release heat to the atmosphere, gain density due to cooling and eventually sink in the subpolar North Atlantic and adjacent Arctic seas thereby generating the return southward flow of colder waters at depths (**Fig. 3**) [Dickson and Brown, 1994; Koltermann et al., 1999]. Temporal variability of the large-scale circulation and associated heat transport in the subpolar North Atlantic is one of the principal factors behind the high-latitude climate anomalies in the Northern Hemisphere.

Progress in understanding the causes of the ongoing climate change and forecasting climate variability in the Arctic and over European part of Russia for the next decades require reliable observation-based estimates of the variability of the North Atlantic circulation and the Atlantic–Arctic heat and freshwater fluxes, as well as elucidation of the underlying mechanisms. In a number of recent studies, radical changes in the thermohaline regime and large-scale circulation in the Atlantic Ocean have been suggested to occur under global warming. For instance, the long-term freshening of the subpolar North Atlantic deep waters since the mid-1960s [Dickson et al., 2002] has been (cautiously) attributed to climate change-related factors [Curry et al., 2003; Hansen et al., 2004]. Hypothetically, under global warming, an increased evaporation in the tropics and increased precipitation at high latitudes, coupled with an intensified melting of Arctic ice, lead to the upper-ocean freshening in the regions of deep water formation and, hence, to the deep water freshening in the Atlantic Ocean. At the same time, milder winters along with the upper-ocean freshening lead to a decrease in the deep water production rates, which results in slowing of the Atlantic Meridional Overturning Circulation [e.g., Hansen et al., 2004; Bryden et al., 2005].

To better understand the past and present changes in the ocean-atmosphere dynamical system, as well as their causes and consequences, data on the full-depth oceanic variability are needed. An indispensable effective tool for assessing the large-scale circulation and thermohaline changes in the deep ocean and investigating mechanisms governing these changes are repeated full-depth transoceanic observations.

Since 1997, the P.P. Shirshov Institute of Oceanology has carried out the long-term monitoring of the North Atlantic circulation and water mass properties in the 59.5°N hydrographic section between Cape Farewell (Greenland) and Scotland (**Fig. 3**). Since 2002, the section has been repeated yearly on board the Russian research vessels, providing high precision data on temperature, salinity, oxygen and nutrients concentrations, and current velocities in the entire water column – “from shore to shore”, from the sea surface to the bottom. In 2011, in addition to annual repeat measurements at 59.5°N, the P.P. Shirshov Institute of Oceanology started full-depth repeat observations of the oceanic exchange between the Atlantic and Arctic oceans through the straits between Greenland, Iceland, Faeroe and Shetland Islands (**Fig. 3**). The full-depth observations – of the same oceanic quantities as at 59.5°N – are performed in the straits from research vessels twice a year, in summer and fall. Based on the unique data set thus collected, a number of fundamental findings have already been achieved. Below, we briefly summarize the main subjects and results of our research.

The 59.5°N transatlantic section (**Fig. 3**) was designed for monitoring the large-scale circulation and thermohaline / chemical properties of oceanic waters at the northern periphery of the NA – the region where the warm upper-ocean waters are transformed by deep convection and mixing into the colder intermediate and deep waters – the Labrador Sea Water (LSW), Iceland

Scotland Overflow Water (ISOW) and Denmark Strait Overflow Water (DSOW) (**Fig. 3**) – transported southward in the lower limb of the Atlantic MOC. Hydrographic data collected at 59.5°N along with those obtained within the framework of the kindred projects, primarily the French OVIDE (http://www.ifremer.fr/lpo/ovide), and historical data sets have been used for studying the dense water production [Falina et al., 2007; Falina et al., 2012], decadal temperature and salinity changes in the intermediate–deep water column [Sarafanov et al., 2007; Sarafanov et al., 2008; Sarafanov et al., 2010b, Gladyshev et al., 2016, Gladyshev et al., 2018], causes of these changes [Sarafanov, 2009; Sarafanov et al., 2010b], the mean state [Sarafanov et al, 2012] and long-term variability of the large-scale circulation in the region [Sarafanov et al., 2009; Sarafanov et al, 2010a; Våge et al., 2011].

1.4.2. Reversal of the deep-water freshening

The LSW and Nordic Seas overflow-derived deep waters, ISOW and DSOW, freshened in the northern North Atlantic during the last three–four decades of the 20th century [Dickson et al., 2002]. Between the 1960s and 1990s, the water column in the region freshened on average by about 0.03 [Curry et al., 2003].

The long-term freshening reversed in the mid-1990s [Sarafanov et al., 2007; Sarafanov et al., 2008; Sarafanov et al., 2010b]. The salinification (and warming) of the intermediate and deep waters since the mid-1990s (**Fig. 5**) was much more intense than the preceding freshening. Over nearly a decade (1997–2006), temperature / salinity in the intermediate–deep water column ($\sigma_0 \geq 27.45$, depths > 500–1000 m) at 59.5°N increased by ~0.3°C / 0.03–0.04 [Sarafanov et al., 2008].

In the Irminger Sea, the long-term freshening in the deep water column (σ_0>27.80, depths > ~2000 m) reversed in the early 2000s [Sarafanov et al., 2010b]. The observed freshening reversal was a lagged consequence of the persistent ISOW salinification that occurred upstream, in the Iceland Basin, after 1996 due to salinification of the northeast Atlantic waters entrained into the overflow. It was demonstrated [Sarafanov et al., 2010b] that the entrainment salinity increase was associated with the North Atlantic Oscillation (NAO)-induced weakening and contraction of the Subpolar Gyre and corresponding northwestward advance of subtropical waters that followed the NAO decline in the mid-1990s and continued through the mid-2000s. Remarkably, the deep water freshening reversal was not related to changes in the overflow water salinity.

1.4.3 Deep convection in the Irminger Sea

The oxygen data collected in 1997 in the northern North Atlantic in several sections ending nearby the southern tip of Greenland provided the observation-based support for the hypothesis [Pickart et al., 2003] that winter convection in the Irminger Sea may penetrate deep into the LSW layer (1000 – 2000 m) thus causing local renewal of this water mass. A separate lateral maximum of oxygen concentrations in the deep LSW layer was detected east of Cape Farewell (59.5°N, 36–40°W): the concentrations increased (by ~0.1 ml/l) from the Labrador Sea eastern edge toward the Irminger Sea (**Fig. 4**) rather than the reverse, as would be expected if LSW observed in the Irminger Sea interior in 1997 were solely of advective origin [Falina et al., 2007].

The section along 59.5 N crosses the northernmost convection site in the Irminger Sea. The northernmost LSW is characterized by relatively high temperature and salinity because of the Irminger Current (the westernmost North Atlantic Current branch) contribution. Its thermohaline variability in 21 century is shown by Gladyshev et al., 2016. The decadal LSW warming and salinification reversed in 2012. Strong and continuous cooling and freshening occurred after 2015 when anomalous convection developed in the Irminger Sea [Gladyshev et al., 2016, Gladyshev et al., 2019].

1.4.4. Deep-ocean salinity changes and the NAO

Close relationship between the thermohaline properties of the northern North Atlantic intermediate and deep waters and the winter NAO index on a decadal time scale ($r^2 \approx 0.65$, 1950s–2000s, **Fig. 6b** and **6c**) was revealed [Sarafanov, 2009] from the observation-based salinity time series for LSW in the Labrador Sea [Yashayaev, 2007] and ISOW in the Iceland basin [Boessenkool et al., 2007; Sarafanov et al., 2007]. Persistent NAO decline (amplification) leads to warming and salinification (cooling and freshening) in the intermediate–deep water column.

An explanation for the close link between the NAO and the coherent decadal changes in the intermediate and deep water properties in the region was proposed [Sarafanov, 2009]. The two factors dominate this link (**Fig. 6d**): (i) intensity of convection in the Labrador Sea controlling injection of relatively cold fresh waters into the intermediate layer and (ii) zonal extent of the Subpolar Gyre that regulates the relative contributions of cold fresh subpolar waters and warm saline subtropical waters to the entrainment into the Norwegian Sea overflow south of the Iceland–Scotland Ridge and to the Atlantic inflow to the Nordic Seas. These factors act in phase leading to the observed coherent thermohaline changes in the intermediate–deep water column.

Due to weakening of the surface forcing associated with the NAO transition into neutral to low phase (1950s to mid-1960s, mid-1990s to mid-2000s), convection in the Labrador Sea weakens diminishing cold fresh water penetration into the intermediate layer. This results in warming and salinification at the intermediate depths in the Subpolar Gyre. Concurrently, the Subpolar Gyre contracts allowing northward advance of warm saline upper-ocean and intermediate subtropical waters in the northeastern North Atlantic. Northward progression of subtropical waters increases temperature and salinity at the upper intermediate levels and, correspondingly, increases temperature and salinity of the northeast Atlantic waters entrained into the Iceland–Scotland overflow along its pathway to the deep Iceland basin. As a result, temperature and salinity at the deep levels increase. The contrary changes – intensification of deep convection in the Labrador Sea and expansion of the Subpolar Gyre – caused by amplifying surface forcing (mid-1960s to mid-1990s) lead to cooling and freshening at the intermediate–deep levels. Additionally, under high-NAO conditions, deep convection may occur in the Irminger Sea potentially contributing to cooling and freshening at the intermediate (LSW) levels. The two regimes of convection and large-scale circulation corresponding to stronger (early 1990s) and weaker (mid-1960s, mid-2000s) NAO-related atmospheric forcing are schematically visualized in **Fig. 7**.

1.4.5 Deep-ocean salinity changes and climate change

There are increasing concerns that in the warmer climate, the MOC may substantially decline due to a decrease in the convective activity in the northern North Atlantic and Nordic Seas [e.g., Meehl et al., 2007]. The long-term freshening in the Nordic Seas and freshening of the northern North Atlantic deep waters in the 1960s–1990s have been considered as a likely indicator or precursor of the dramatic change in the MOC [e.g., Hansen et al., 2004]. The freshening has been attributed to a combination of factors potentially associated with the global warming: the increasing ice melt and net precipitation at high latitudes [e.g., Curry et al., 2003]. A probable causality between the climate change and the decreasing North Atlantic deep water salinity has supported the concerns and unfavorable predictions, thus 'warming up' the reasonable scientific debate on climate change and overblown speculations in media.

Despite the long-term increase in freshwater input to the Arctic, freshening in the northern North Atlantic had reversed in the mid-1990s, as we demonstrated above. This reversal forces us to revise the hypotheses on the mechanisms behind the deep-water thermohaline anomalies. It seems doubtful that the persistent global temperature growth may lead to the opposite decadal trends (positive-then-negative-then-positive, **Fig. 6**) in the deep water salinity.

Our results [Sarafanov et al., 2008; Sarafanov, 2009; Sarafanov et al., 2010b] suggest that natural atmospheric variability over the North Atlantic plays the major role in the deep-water thermohaline variability on a decadal time scale. There are no reasons to associate the deep-water freshening in the 1960s–1990s with climate change, unless the 3-decade-long surface forcing amplification is evidently shown to be a consequence of the latter. Having said that, the net 1950s–2000s trends in the water mass salinities are negative implying that the global factors (e.g., probable intensification of hydrological cycle [Curry et al., 2003]) may act on longer time scales.

1.4.6 Decadal variability of the Deep Western Boundary Current at Cape Farewell

Recent decadal changes in the Deep Western Boundary Current (DWBC) transport southeast of Cape Farewell were assessed from hydrographic data (1991–2007, **Fig. 7a**), direct velocity measurements (2002–2006) and satellite altimetry (1992–2007). Following the approach used in earlier studies [e.g., Bacon, 1998], we first determined that the DWBC (σ_0>27.80) baroclinic transport (T_{BC}) referenced to 1000 m depth increased by ~2 Sv between the mid-1990s (1994–1997) and 2000s (2000–2007) (**Fig. 8b**) [Sarafanov et al., 2009]. In the next step, we quantified velocity changes at the reference level (1000 m) by combining estimates of the hydrography-derived velocity changes in the water column and the altimetry-derived velocity changes at the sea surface [see Sarafanov et al., 2010a]. The inferred increase in the southward velocity at 1000 m above the DWBC in 1994–2007 indicates that the increase in the DWBC absolute transport was larger but very close to the 2-Sv increase in the DWBC T_{BC}. This result along with the observed coherence of the DWBC absolute and baroclinic transport changes between individual observations [Sarafanov et al., 2010a] imply that the DWBC absolute transport variability in the region is well represented by its baroclinic component on decadal and shorter time scales.

The historical record of the DWBC T_{BC} (1955–2007, **Fig. 8c**) updated after Bacon [1998] shows distinct decadal variability (±2–2.5 Sv) with the transport minima in the 1950s and mid-1990s, maximum in the early 1980s and moderate-to-high transport in the 2000s. The DWBC T_{BC} decadal variability is consistent with the general pattern of the recent decadal hydrographic and circulation changes in the northern North Atlantic. The DWBC T_{BC} anomalies negatively correlate (R = –0.80, 1955–2007) with thickness anomalies of the Labrador Sea Water (LSW) at its origin implying a close link between the DWBC transport southeast of Cape Farewell and the LSW production in the Labrador Sea (**Fig. 8d**). During the recent three decades (late 1970s – late 2000s), the DWBC T_{BC} changes were also in-phase with changes in the strength and zonal extent of the Subpolar Gyre [see Sarafanov et al., 2010a]. In particular, the Gyre weakening at shallow levels in the mid-1990s – mid-2000s was accompanied by the DWBC strengthening in the Irminger Sea [Sarafanov et al., 2009; Sarafanov et al., 2010a; Våge et al., 2011]. The results imply that the decadal changes in the (i) LSW production, (ii) SPG strength and (iii) DWBC transport in the Irminger Sea are linked, representing a complex coherent oceanic response to the decadal variability of the surface forcing.

1.4.7 Mean state of the full-depth circulation in the 2000s

A mean state of the full-depth summer circulation in the Atlantic Ocean in the region in between Cape Farewell (Greenland), Scotland and the Greenland-Scotland Ridge (see **Fig. 3**) was assessed by combining 2002–2008 yearly hydrographic measurements at 59.5°N, mean dynamic topography, satellite altimetry data and available estimates of the Atlantic–Nordic Seas exchange [see Sarafanov et al., 2012]. The mean absolute transports by the upper-ocean, mid-depth and deep currents and the MOC ($MOC\sigma$=16.5±2.2 Sv, at σ_0=27.55) at 59.5°N were quantified in the density space. Inter-basin and diapycnal volume fluxes in between the 59.5°N section and the Greenland-Scotland Ridge were then estimated from a box model.

The estimated meridional and diapycnal volume fluxes contributing to the MOC are schematically visualized in **Fig. 9**. The dominant components of the meridional exchange across 59.5°N are the North Atlantic Current (NAC, 15.5±0.8 Sv, σ_0<27.55) east of the Reykjanes Ridge, the northward Irminger Current (IC, 12.0±3.0 Sv) and southward Western Boundary Current (WBC, 32.1±5.9 Sv) in the Irminger Sea and the deep water export from the northern Iceland Basin (3.7±0.8 Sv, σ_0>27.80). About 60% (12.7±1.4 Sv) of waters carried in the $MOC\sigma$ upper limb (σ_0<27.55) by the NAC/IC across 59.5°N (21.1±1.0 Sv) recirculates westwards south of the Greenland-Scotland Ridge and feeds the WBC. 80% (10.2±1.7 Sv) of the recirculating NAC/IC-derived upper-ocean waters gains density of σ_0>27.55 and contributes to the MOCσ lower limb. Accordingly, the contribution of light-to-dense water conversion south of the Greenland-Scotland Ridge (~10 Sv) to the MOCσ lower limb at 59.5°N is one and a half times larger than the contribution of dense water production in the Nordic Seas (~6 Sv).

1.4.8 Cascading of dense shelf waters in the Irminger Sea

Based on the hydrographic data collected at 59.5°N, 64.3°N and 65–66°N in the western Irminger Sea in the 1990s – 2000s, an observational evidence for the deep-reaching cascading of dense shelf waters south of the Denmark Strait was found [Falina et al., 2012]. The data collected in the northwestern Irminger Sea (65–66°N) indicate that the East Greenland Current ~200 km south of the Denmark Strait occasionally carries shelf waters as dense as the overflow-derived deep waters transported by the DWBC (σ_0 > 27.80). Hydrographic traces of cascading of dense shelf waters down the East Greenland slope were found from repeat measurements at 64.3ºN, where the densest fresh plumes were observed within the DWBC (σ_0 > 27.80) (**Fig. 10**). Using the data collected at 59.5°N, we showed that the fresh 'signals' originating from the shelf can be traced in the DWBC as far downstream as the latitude of Cape Farewell, where the anomalously fresh oxygenated plumes are repeatedly observed in the ISOW and DSOW density classes.

The results of our analysis along with the results from earlier studies [e.g., Rudels et al., 1999; Rudels et al., 2002] indicate that shelf water cascading in the northern Irminger Sea is an intermittent process occurring in all seasons of the year. This implies that, despite the apparent short duration of a particular cascading event, the cumulative contribution of such events to the thermohaline variability and southward export of the deep waters in the WBC can be considerable. Our tentative estimate based on data from two synoptic surveys at ~59.5°N suggests that the transient contribution of a cascading event in the northern Irminger Sea to the DWBC transport at Cape Farewell can be as large as ~25%.

References

1. Bacon, S. (1998), Decadal variability in the outflow from the Nordic seas to the deep Atlantic Ocean, *Nature*, *394*, 871–874.
2. Boessenkool, K. P., Hall, I. R., Elderfield, H., and I. Yashayaev (2007), North Atlantic climate and deep-ocean flow speed changes during the last 230 years, *Geophys. Res. Lett.*, *34*, L13614, doi:10.1029/2007GL030285.
3. Curry, R., Dickson, R., and I. Yashayaev (2003), A change in the freshwater balance of the Atlantic Ocean over the past four decades, *Nature*, *426*, 826–829.
4. Dickson, R. R., and J. Brown (1994), The production of North Atlantic Deep Water: Sources, rates and pathways, *J. Geophys. Res.*, *99*, C6, 12319–12341.
5. Dickson, R., Yashayaev, I., Meincke, J., Turrell, B., Dye, S., and J. Holfort (2002), Rapid freshening of the deep North Atlantic Ocean over the past four decades, *Nature*, *416*, 832–837.
6. Falina, A., A. Sarafanov, and A. Sokov (2007), Variability and renewal of Labrador Sea Water in the Irminger Basin in 1991–2004, *J. Geophys. Res.*, *112*, C01006, doi: 10.1029/2005JC003348.
7. Falina A., A. Sarafanov, H. Mercier, P. Lherminier, A. Sokov, and N. Daniault (2012), On the cascading of dense shelf waters in the Irminger Sea, *J. Phys. Oceanogr.*, doi:http://dx.doi.org/10.1175/JPO-D-12-012.1.
8. Gladyshev S., V. Gladyshev, A. Falina, A. Sarafanov (2016), Winter convection in the Irminger Sea in 2004-2014, *Oceanology,* V. 56*,* N 3, P. 326-335, doi*:* 10.1134/S0001437016030073.
9. Gladyshev S., V. Gladyshev, S. Gulev, A. Sokov (2016), Anomalously deep convection in the Irminger Sea during the winter of 2014–2015, *Doklady Earth Sciences,* V.469, Part I, P. 766-770, doi: 10.1134/S1028334X16070229.
10. Gladyshev S., V. Gladyshev, L. Pautova, S. Gulev, A. Sokov (2018), Intermediate waters in the Irminger Sea during deep convection: variability and the role of circulation mechanisms, *Doklady Earth Sciences*, V. 483, Part II, P. 1553-1557, doi: 10.1134/S1028334X18120127.
11. Hansen, B., Osterhus S., Quadfasel D., and W. Turrell (2004), Already the day after tomorrow?, *Science*, *305*, 953–954.

12. Hurrell, J. W. (1995), Decadal trends in the North Atlantic Oscillation: regional temperatures and precipitation, *Science*, *269*, 676–679.

13. Koltermann, K. P., A. Sokov, V. Tereschenkov, S. Dobroliubov, K. Lorbacher, and A. Sy (1999), Decadal changes in the thermohaline circulation of the North Atlantic, *Deep Sea Res.*, *Part II*, *46*, 109–138, doi:10.1016/S0967-0645(98)00115-5.

14. Lherminier, P., H. Mercier, T. Huck, C. Gourcuff, F. F. Perez, P. Morin, A. Sarafanov, and A. Falina (2010), The Atlantic Meridional Overturning Circulation and the subpolar gyre observed at the A25–Ovide section in June 2002 and 2004, *Deep-Sea Res.*, *Part I*, *57*, 1374–1391, doi:10.1016/ j.dsr.2010.07.009.

15. Meehl, G. A., (2007), Global climate projections. Climate Change 2007: The Physical Science Basis, S. Solomon et al., Eds., Cambridge University Press, 747–847.

16. Pickart, R. S., Spall, M., Ribergaard, M. H., Moore, G. W. K. and R. Milliff (2003), Deep convection in the Irminger Sea forced by the Greenland tip jet, *Nature*, *424*, 152–156.

17. Rudels B., Eriksson P., Grönvall H., Hietala R. and Launiainen J. (1999), Hydrographic Observations in Denmark Strait in Fall 1997, and their Implications for the Entrainment into the Overflow Plume, *Geophys. Res. Lett.*, *26*, 1325–1328.

18. Rudels, B., E. Fahrbach, J. Meincke, G. Budeus, and P. Eriksson (2002), The East Greeenland Current and its contribution to the Denmark Strait overflow, *ICES J. Marine Science*, *59*, 1133–1154.

19. Sarafanov, A., A. Sokov, A. Demidov, and A. Falina (2007), Warming and salinification of intermediate and deep waters in the Irminger Sea and Iceland Basin in 1997–2006, *Geophys. Res. Lett.*, *34*, L23609, doi:10.1029/2007GL031074.

20. Sarafanov, A., A. Falina, A. Sokov, and A. Demidov (2008), Intense warming and salinification of intermediate waters of southern origin in the eastern subpolar North Atlantic in the 1990s to mid-2000s, *J. Geophys. Res.*, *113*, C12022, doi:10.1029/2008JC004975.

21. Sarafanov, A. (2009), On the effect of the North Atlantic Oscillation on temperature and salinity of the subpolar North Atlantic intermediate and deep waters, *ICES J. Marine Science*, *66 (7),* 1448–1454, doi:10.1093/icesjms/fsp094.

22. Sarafanov, A., A. Falina, H. Mercier, P. Lherminier, and A. Sokov (2009), Recent changes in the Greenland–Scotland overflow-derived water transport inferred from

hydrographic observations in the southern Irminger Sea, *Geophys. Res. Lett.*, *36*, L13606, doi:10.1029/2009GL038385.

23. Sarafanov A., A. Falina, P. Lherminier, H. Mercier, A. Sokov, and C. Gourcuff (2010a), Assessing decadal changes in the Deep Western Boundary Current absolute transport southeast of Cape Farewell (Greenland) from hydrography and altimetry, *J. Geophys. Res.*, *115*, C11003, doi:10.1029/2009JC005811.

24. Sarafanov A., H. Mercier, A. Falina, A. Sokov, and P. Lherminier (2010b), Cessation and partial reversal of deep water freshening in the northern North Atlantic: observation-based estimates and attribution, *Tellus*, *62A*, 80–90, doi:10.1111/j.1600-0870.2009.00418.x.

25. Sarafanov A., A. Falina, H. Mercier, A. Sokov, P. Lherminier, C. Gourcuff, S. Gladyshev, F. Gaillard, and N. Daniault (2012) Mean full-depth summer circulation and transports at the northern periphery of the Atlantic Ocean in the 2000s, *J. Geophys. Res., 117,* C01014, doi:10.1029/2011JC007572.

26. Schmitz, W. J., Jr., and M. S. McCartney (1993), On the North Atlantic Circulation, *Rev. Geophys.*, *31*, 29–49.

27. Schott, F. A., and P. Brandt (2007), Circulation and deep water export of the subpolar North Atlantic during the 1990s, *in Ocean Circulation: Mechanisms and Impacts*, *Geophys. Monograph Series*, *173*, Eds. A. Schmittner, J. Chiang, and S. Hemmings, 91–118, doi:10.1029/173GM08.

28. Sutherland, D. A., and R. S. Pickart (2008), The East Greenland Coastal Current: structure, variability, and forcing, *Prog. Oceanogr.*, *78*, 58–77, doi:10.1016/j.pocean.2007.09.006.

29. Våge K., R. Pickart, A. Sarafanov, Ø. Knutsen, H. Mercier, P. Lherminier, H. van Aken, J. Meincke, D. Quadfasel, and S. Bacon (2011a), The Irminger Gyre: circulation, convection, and interannual variability, *Deep-Sea Res. Part I*, *58*, 590–614, doi:10.1016/j.dsr.2011.03.001.

30. van Aken, H. M. (2007), The oceanic thermohaline circulation: An introduction, New York, Springer, 326 p., ISBN 978-0-387-36637-1.

31. Yashayaev, I. (2007), Hydrographic changes in the Labrador Sea, 1960–2005, *Prog. Oceanogr.*, *73*, 242–276.

1.5 Preliminary Results

The upper-ocean, mid-depth and deep water circulation patterns, merging the results of the present analysis with those from the earlier studies [e.g., *Macrander et al.*, 2005; *Østerhus et al.*, 2005, 2008; *Schott and Brandt*, 2007; *Sutherland and Pickart*, 2008; *Lherminier et al.*, 2010; *Våge et al.*, 2011], are schematically visualized **Fig. 3**. A schematic diagram of the meridional overturning circulation in the Atlantic Ocean north of 59.5°N is displayed in **Fig. 9**.

The results provide the following conceptual view of the gyre / overturning circulation at the northern periphery of the Atlantic Ocean in the 2000s.

The NAC and IC collectively carry 21.1 ± 1.0 Sv of warm upper-ocean waters across 59.5°N northwards within the MOCσ upper limb ($\sigma_0 < 27.55$). About 40% of this flow forms the Atlantic Inflow to the Nordic Seas, and 60% (12.7 ± 1.4 Sv) recirculates westwards in the subpolar gyre northern limb south of Iceland to feed the WBC in the Irminger Sea. Only 20% (2.4 ± 1.2 Sv) of the recirculating NAC/IC-derived waters exits the Irminger Sea in the WBC at shallow levels ($\sigma_0 < 27.55$), while 80% (10.2 ± 1.7 Sv, a half of the NAC/IC northward flow across 59.5°N) gains density of $\sigma_0 > 27.55$ and enters the MOCσ lower limb. The resulting net southward transport in the MOCσ lower limb at the latitude of Cape Farewell is 16.5 ± 2.2 Sv, of which ~60% (~10.2 Sv) is due to light-to-dense water transformation south of the GSR.

As no dense-to-light water re-conversion is expected to occur in the subpolar gyre, the NAC/IC-derived waters, once entering the MOCσ lower limb in the Irminger Sea, will eventually contribute to the MOCz lower limb (~11 Sv at 59.5°N) at the southern margin of the subpolar region. There, at ~48°N, the MOCσ and MOCz are of nearly the same magnitude, 16 ± 2 Sv, as estimated from data collected in the 1990s [see *Schott and Brandt*, 2007; *Lumpkin et al.*, 2008]. This is very close to our estimate of the mean MOCσ at 59.5°N. The comparison is tentative, though, because it does take into account the decadal variability of the MOC [*Koltermann et al.*, 1999; *Willis*, 2010]. With this caveat in mind, our results imply a minor contribution to the MOCσ by the net dense water formation in the subpolar gyre between ~48°N and 59.5°N. This inference concurs with the results by *Pickart and Spall* [2007] suggesting a minor contribution to the Atlantic MOC by the net water mass transformation in the Labrador Sea.

To conclude, the results of the present study, verified with independent estimates where possible, provide the first observation-based quantitative view of a mean state of the gyre / overturning circulation at the northern periphery of the Atlantic Ocean. The most interesting features of the obtain circulation pattern are as follows:

• Nearly half of volume of the upper-ocean waters transported northward across 59.5°N in the eastern limb of the subpolar gyre (NAC and IC, $\sigma_0 < 27.55$) overturns in the density plane south of the GSR and feeds the lower limb of the Atlantic MOCσ.

• The contribution to the MOCσ lower limb at 59.5°N by overturning (light-to-dense transformation) of the NAC / IC-derived upper-ocean waters south of the GSR is one and a half times as large as the contribution of the Nordic Seas overflows.

• The net southward flow in MOCσ lower limb at 59.5°N is associated primarily with the deep water ($\sigma_0 > 27.80$) export. Nearly half of the net southward flow of deep waters across 59.5°N is due to entrainment of the Atlantic waters in the Irminger Sea.

• The DWBC at 59.5°N is fed primarily by the Denmark Strait Overflow and by the diapycnal flux / entrainment from the mid-depth layer, while the contribution to the DWBC transport from the ISOW flow is minor. A major part of the ISOW transported into the Irminger Sea from the Charlie-Gibbs Fracture Zone recirculates southward in the eastern Irminger Sea and exits the basin via an interior pathway rather than along the western boundary. The results can be used for validation of numerical models. From this perspective, multi-year mean transports have an obvious advantage over individual section-based synoptic estimates, which bear the impress of vigorous variability occurring on a variety of spatial and temporal scales. The methodological outcome is that the combined use of repeat hydrography, the MDT by *Rio and Hernandez* [2004] and satellite altimetry data can provide a useful estimate of the mean full-depth circulation across a transatlantic section without imposing *a priori* constraints.

1.6 Major Problems and Goals Not Achieved

OS75 kHz VM ADCP stopped recording of data few times during cruise because of MRU 3 problem and repeated program rebooting took 5-15 minutes.

2. CONTINUOUS MEASUREMENTS (on station and underway)

2.1 Navigation

Navigation data from Trimble SPS 855/555H GPS was recorded every 1 second and was stored on the PC in binary format.

2.2 Meteorological Measurements

The standard meteorological measurements were stored in the separate files on the same PC with navigation data. Recording were running immediately after departure from Arkhangelsk (Russia) on 8 August, and worked reliably until completion of the cruise in Arkhangelsk (Russia) on 15th September. Variability of the atmospheric pressure and air temperature during transatlantic section are shown in **Figures 11-12**.

2.3 Echosounding

The bathymetric equipment aboard during RV *Akademik Mstislav Keldysh* cruise 77 consists of EA600 12 kHz hydrographic echosounder. Data were collected for most of the cruise. The Hull mounted transducer is located 5.8 metres below the sea surface and this value was entered to estimate the depth.

Depth was indicated on the echosounder display and stored on the PC together with the navigation.

2.4 Vessel Mounted Acoustic Doppler Current Profiler (VMADCP) OS 75 kHz

The Ocean Surveyor 75 kHz is designed for vessel-mount current profile measurement in the upper ocean water from depths greater than 30-50 meters. The system consists of a transducer and electronics chassis connected to PC. Data are transmitted in binary format through the I/O cable. GPS data in NMEA format are transmitted separately to another PC COM – port. The VMADCP can operate in two regimes (Narrow Bandwith and Broad Bandwith Profiling). The Broad Bandwith Profiling was used during the cruise. Its main specifications are shown below.

To collect OS 75 kHz data we used *VmDas* software (version 1.48). The NMEA messages *VmDas* reads are standard GGA, HDG, HDT, VTG messages.

Broad Band (high-precision mode)	Bin size	Maximum range	Accuracy (cm/s)
	16 m	350 - 450 m	7

We used a following configuration to collect the data.

WP00001 – Broad Bandwidth profiling

WN045 – number of bins 45

WF1600 – blanking size 16 m

BP00 – no bottom track (BP),

BP01 – bottom track (BP),

VmDas saves data in a few files with extension ENX, ENS, ENR (raw data with and without navigation), NR – NMEA messages, STA and LTA averaged data. Misalignment angle was introduced in configuration file and was used by VmDas for data correction.

Data processing performed STA files with 40-profile averaging. Taking into account that single ping takes about 3 seconds, one 40-profile ensemble lasts near 120 seconds in Narrow Bandwidth regime.

Data processing consists of data conversion in NetCDF format with extension NC and further cleaning, filtering, tide removing (using barotropic tidal model TPXO 7.2) and averaging. The standard averaging was 3 km. IFREMER software was used to process OS 75 kHz data.

3. ON-STATION MEASUREMENTS

3.1 CTD

3.1.1 Equipment

The deep profiler system used during the cruise included the following components: SBE 32 painted aluminum 24 bottle multisampler frame, SBE 9P-0727 and 1277 CTDs, Up and Down looking (WHS -300 kHz) RD Instruments Acoustic Doppler Current Profiler (LADCP), Separate Battery pack pressure case ext. 6000 m connected to LADCPs with star cable, 22 x 5 liter Test Oceanic Niskin bottles, Benthos altimeter PSA-900D.

Lab equipment for data acquisition and archiving of CTD/LADCP data consisted of the following items mounted on the deck. Shuttle XH310V/Intel Core i5-8400/16Гб Ram/240Гб SSD. APC Back-UPS 550VA/330W, SBE 11p Deck Unit.

Cruise Preparation

Equipment and sensors were assembled when the ship crossed the Baltic and North Seas (24-27th June). Water bottles were checked for integrity of seals, taps, stoppers and lanyards before being fitted and roped to the multisampler frame.

Deployment

The CTD was deployed with a lowering rate of 60 meters/min (30-40 meters/min in the upper 200 meters or deeper if the conditions are rough). It is recovered at a rate of 60 meters/min.

The LADCPs fitted within the frame with a separate battery pressure case performed well. These units contain a compass and tilt sensors which could possibly provide useful information on the attitude and rotation of the whole profiler package throughout deployments.

Bottle firing using the deck unit and pylon was very reliable during the cruise.

Operationally this has been a successful cruise with virtually no time being lost due to mechanical or equipment failure.

3.1.2 Data processing and calibration

CTD data were logged at 24 scans per second and passed from the CTD deck unit to the PC.

The CTD data was recorded onto disk by the PC using SEABIRD SEASOFT-Win 32: Seasave 7, Software Release 7.21d. A screen display of temperature, oxygen, salinity and density profiles vs pressure are used to decide the depths at which bottles are to be tripped on the up cast. The bottles are tripped using the enable and fire buttons on the PC screen. During post-processing, the SEASAVE software stores 35 scans at each bottle trip within a separate file. At the end of the station, all the data and header files associated with the station are transferred immediately via ethernet to the second PC. The SBE data processing software is used to create 1 dbar processed data files.

The data processing takes the following steps:

DATCNV Converts the raw data to physical parameters.

WILDEDIT For every block of 100 scans, flags all scans whose pressure, temperature, conductivity and oxygen values differ from the mean by more than 2 standard deviations. Recomputes mean from unflagged data then marks as bad all scans exceeding 20 standard deviations from these new values.

FILTER Low pass filter pressure channel with time constant used for pressure 0.150 seconds.

ALIGNCTD Aligns the oxygen values relative to the pressure values accounting for the time delays in the system. Time offsets of 4.000 secs for oxygen are used.

CELLTM A recursive filter used to remove the thermal mass effects from the conductivity data. Thermal anomaly amplitude and time constants of 0.0300 and 7.0000 were used.

LOOPEDIT Marks as bad, all cycles on the down trace for which the vertical velocity of the CTD unit is less than 0.25 metres/sec.

WINDOW FILTER cosine filter temperature and conductivity, window size 23 scans.

DERIVE Computes salinity, potential temperature, sigma-t, sigma theta and oxygen values.

BINAVG Averages the down cast into 1 dbar pressure bins.

SPLIT Splits the data into DOWN and UP cast.

Calibration data

The CTD calibrations used during this cruise were supplied by Sea Bird Electronics and are as follows:

Pre-cruise calibration:
CALIBRATION DATE: 12-Aug-16 (all stations)
Conductivity Sensor S/N 044580
G= -9.90055574e+000
H=1.24515002e+000
I=-1.59442188e-005
J=5.25554824e-005

CPcor=-9.57000000e-008
CTcor=3.2500e-006

Pre-cruise calibration:
CALIBRATION DATE: 09-Aug-16 (all stations)
Temperature Sensor S/N 0360082
Temperature ITS-90 = 1/{g + h[*ln*(f0/f)] + i[*ln*2(f0/f)] + j[*ln*3(f0/f)]} - 273.15 (°C)
Following the recommendation of JPOTS: T68 is assumed to be 1.00024 * T90 (-2 to 35°C)
f is the frequency
G=4.33833475e-003
H=6.37459433e-004
I=2.21244493e-005
J=2.06389145e-006
F0=1000.000

Pressure Sensor S/N 1277 **(all stations) no drift**
CALIBRATION DATE: 08-Apr-16
C1=-4.312077e+004
C2=-1.722110e-002
C3=1.209000e-002
D1=3.629600e-002
D2=0.000000e+000
T1=3.045887e+001
T2=-2.990540e-004
T3=3.939190e-006
T4=2.543630e-009
Slope=1.00000000
Offset=0.00000
T5=0.000000e+000
AD590M=1.282540e-002
AD590B=-9.419870e+000
Slope = 1.00000
Offset = 0.0 (dbars)

Oxygen Sensor 433321
CALIBRATION DATE: 30-Mar-16 (All Stations)

Soc=4.5081e-001
Offset=-0.4758
A=-3.3789e-003
B= 1.2319e-004
C=-1.7238e-006
D0=2.5826e+000
D1=1.92634e-004
D2=-4.64803e-002
E=3.6000e-002
Tau20=1.5500
H1=-3.3000e-002
H2=5.0000e+003
H3=1.4500e+003

3.1.3 Final Post-Cruise CTD Calibrations

Temperature Calibration Temperature Sensor 036082

0.0000 sensor drift was applied to the temperature data based on the *pre cruise calibration coefficients* for all stations.

Pressure Calibration Pressure Sensor S/N 131735

Final CTD pressure correction: Since no drift for pressure sensor was defined by SeaBird Electronics pressure was corrected for atmospheric pressure only. With offset in *.con* or *.xmlcon* file set to -0.0026 db, pressure measured by CTD should equal barometric pressure

• Calculate offset (db) = barometer reading – CTD reading

– Conversion of psia to decibars: decibars = (psia - 14.7) * 0.6894759

• Enter calculated offset in *.con* or *.xmlcon* file

• Example:

– CTD reads -2.5 dbars

– Barometer reads 14.65 psia.

Converting to decibars, barometer reads (14.65 - 14.7) * 0.6894759 = -0.034 dbars

– offset (db) = barometer reading – CTD reading = -0.034 - (-2.5) = 2.466

Salinity Calibration Conductivity Sensor 044580

We used *pre-cruise calibration coefficients* with slope correction according to App. Notes No 31 (Revised February 2010).

If **α** is the conductivity computed from the **pre-cruise bath data** (temperature and frequency) using **post-cruise calibration coefficients** and **β** is the true conductivity in the **pre-cruise bath**, then:

$$\textbf{postslope} = \frac{\sum_{i=1}^{n} (\alpha_i)(\beta_i)}{\sum_{i=1}^{n} (\alpha_i)(\alpha_i)} \qquad \text{(postslope is typically < 1.0)}$$

Sea-Bird calculates and prints the value for postslope on the conductivity calibration sheet for all calibrations since February 1995 (see *Appendix I: Example Conductivity Calibration Sheet*)

To correct conductivity data taken between pre- and post-cruise calibrations:

islope = 1.0 + (b / n) [(1 / postslope) - 1.0]

where

islope = interpolated slope; this is the value to enter in the configuration (.con or .xmlcon) file
b = number of days between pre-cruise calibration and the cast to be corrected
n = number of days between pre- and post-cruise calibrations
postslope = slope from calibration sheet as calculated above (see *Appendix I: Example Conductivity Calibration Sheet*)

In the configuration (.con or .xmlcon) file, use the **pre-cruise calibration coefficients** and use **islope** for the value of slope.*

Note: In our SEASOFT V2 suite of programs, edit the CTD configuration (.con or .xmlcon) file using the Configure Inputs menu in Seasave V7 (real-time data acquisition software) or the Configure menu in SBE Data Processing (data processing software).

For typical conductivity drift rates (equivalent to -0.003 PSU/month), islope does not need to be recalculated more frequently than at weekly intervals.

3.1.4 SBE 43 Dissolved Oxygen Sensor Calibration using Winkler Titrations

We use a method for statistically estimating calibration coefficients for calculating dissolved oxygen in milliliters per liter from SBE 43 output voltage. The technique requires dissolved oxygen concentration in ml/l (determined from Winkler titration of water samples) and SBE 43 oxygen voltage outputs at the times the water samples were collected. Sea-Bird's data processing software, SBE Data Processing, is used to produce a data table suitable for the analysis.

Background

The equation used in Sea-Bird's software for calculating dissolved oxygen in ml/l from SBE 43 output voltage is a form of that given in Owens-Millard (1985):

$$Oxygen\ (ml/l) = \left\{Soc * \left(V + Voffset + tau(T,P) * \frac{\partial V}{\partial t}\right)\right\} * Oxsol(T,S) * \left(1.0 + A*T + B*T^2 + C*T^3\right) * e^{\left(\frac{E*P}{K}\right)} \qquad eqn\ 1$$

where:

- V = SBE 43 output voltage signal (volts)
- $\partial V/\partial t$ = time derivative of SBE 43 output signal (volts/second), computed over a default window of 2 seconds
- T = CTD temperature (°C)
- S = CTD salinity (psu)
- P = CTD pressure (dbars)
- K = CTD temperature (°K = °C + 273.15)
- *tau(T,P)* = sensor time constant at temperature and pressure
- *Oxsol(T,S)* = oxygen solubility function (ml/L), which converts oxygen partial pressure (sensor measurement) to oxygen concentration (*Garcia and Gordon, 1992*). See Appendix A in *Application Note 64: Background Information, Deployment Recommendations, and Cleaning and Storage* for values at various temperatures and salinities.
- *Soc, Voffset, A, B, C, E*, and *tau20, D1, D2* [terms in calculation of *tau (T,P)*] are calibration coefficients

The SBE 43 is expected to provide an output voltage that is linear with respect to oxygen concentration. Normal calibration drift manifests itself as a loss of sensitivity and is evident as a change of slope (and less so in offset) in the linear relationship between oxygen concentration and voltage output. The coefficients *A, B, C,* and *E* correct for small secondary responses to temperature and pressure. Because these coefficients change very slowly over time, the values given on the SBE 43 calibration certificate will be used in this analysis, and we will concern ourselves with estimating changes in the slope (Soc) and offset (Voffset).

Setting $\frac{\partial V}{\partial t}$ to zero, we rearrange equation 1 into a linear form and perform a linear regression to obtain a new *Soc* and *Voffset*.

Let:

$$\phi = Oxsol(T,S) * \left(1.0 + A*T + B*T^2 + C*T^3\right) * e^{\left(\frac{E*P}{K}\right)} \qquad eqn\ 2$$

The oxygen equation then reduces to the form in equation 3:

$$Oxygen(ml/l) = Soc * (V + Voffset) * \phi \qquad eqn\ 3$$

This may be expressed in a linear form in equation 4.

$$\frac{Oxygen(ml/l)}{\phi} = Soc * (V + Voffset) = M * V + B \qquad eqn\ 4$$

Where:

Soc = M
Voffset = B / M

A linear regression is calculated using Winkler oxygen concentration divided by ϕ as the dependent variable and SBE 43 output voltage as the independent variable.

Winkler oxygen divided by φ versus SBE 43 output voltage for this cruise is shown in **Fig. 13** and include linear regression lines calculated from the data.

The final coefficients are for the transatlantic section (sta 6283 – 6308)
Soc=4.6839e-001
Offset=-0.3378
469 oxygen samples were used to build this linear fit.

sta 6309-6331
Soc=4.3536e-001
Offset=-0.4726
492 oxygen samples were used to build this linear fit.

The final coefficients are for the DS experiment II (sta 6332 – 6445)
Soc=4.4445e-001
Offset=-0.5196
906 oxygen samples were used to build this linear fit for sill sections.

Procedure

The linear regression that yields a new *Soc* and *Voffset* may be accomplished with spreadsheet software, a hand-held calculator with statistical capability, or (with perseverance) a calculator, graph paper, and pencil. As a first step, extract pressure, temperature, salinity, oxygen saturation, and SBE 43 voltage from the parts of your CTD data collected when the water sampler closures occurred.

Run SBE Data Processing, and select Data Conversion in the Run menu. Select the appropriate configuration (*.con*) and data (*.dat* or *.hex*) files on the *File Setup* tab. Click the *Data Setup* tab and set *Convert data from* to *Upcast and downcast* and *Create file types* to *Create bottle (.ros) file only*.

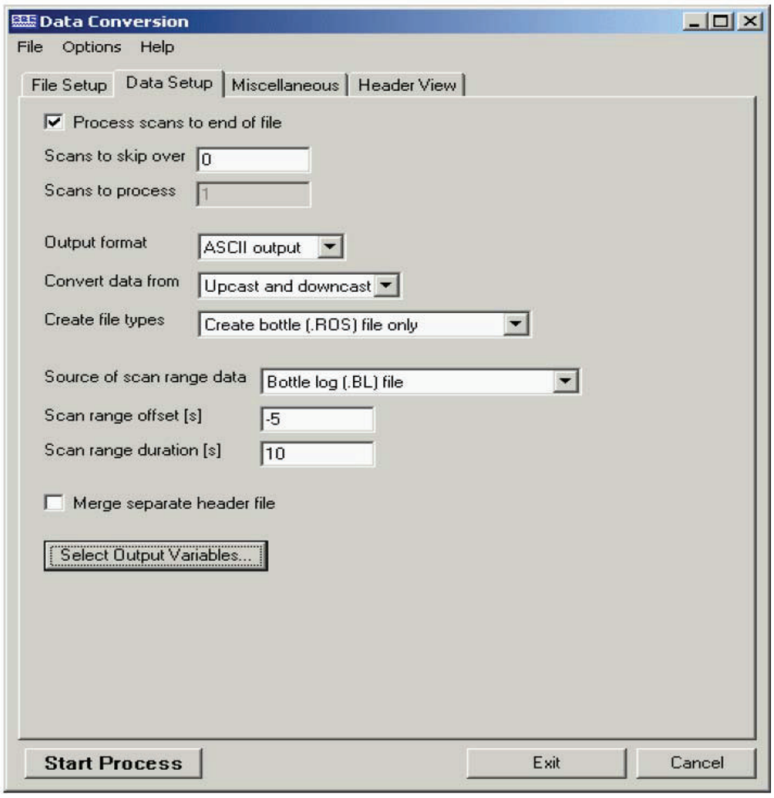

To extract CTD data concurrent to the water sampler closures, Data Conversion must know when the closures occurred. Select an appropriate *Source of scan range data*, depending on your instrument type and how the sampler was commanded to close bottles:

- SBE 9*plus* with SBE 11*plus* or 17*plus* - The data stream is marked with a *bottle confirm* bit each time a closure occurred.
- Using SEASAVE to operate the water sampler - A *.bl* file, with scan ranges corresponding to closures, is created during the cast.
- SBE 19, 19*plus*, 19*plus* V2, or 25 with Auto Fire Module (AFM) and SBE 32 Carousel Water Sampler, or operated autonomously with SBE 55 ECO Water Sampler - The *.afm* file contains scan ranges.

Like all sensors, the SBE 43 has a finite response time to a change in dissolved oxygen concentration. This response time is usually on the order of 6 seconds. For this reason, good sampling procedure dictates that the instrument package should be stopped in the water column long enough for the SBE 43 and all other sensors to completely equilibrate before closing the water sampler. An equilibration time of 5 to 6 response times, or 30 to 36 seconds, is adequate.

In the example above, Data Conversion will begin extracting data 5 seconds before each water sampler closure (*Scan range offset = -5 s*) and will extract a total of 10 seconds of data (*Scan range duration = 10 s*). Note that 10 seconds is longer than the SBE 43 response time. Because we are extracting data for 5 seconds after the water sampler closure, the instrument package must remain stopped for at least this long.

To estimate *Soc* and *Voffset*, you need pressure, temperature, salinity, oxygen saturation (ml/l), and SBE 43 Oxygen Voltage to go with each Winkler titration data value. Click *Select Output Variables* and add each of the required parameters; the dialog box is shown below.

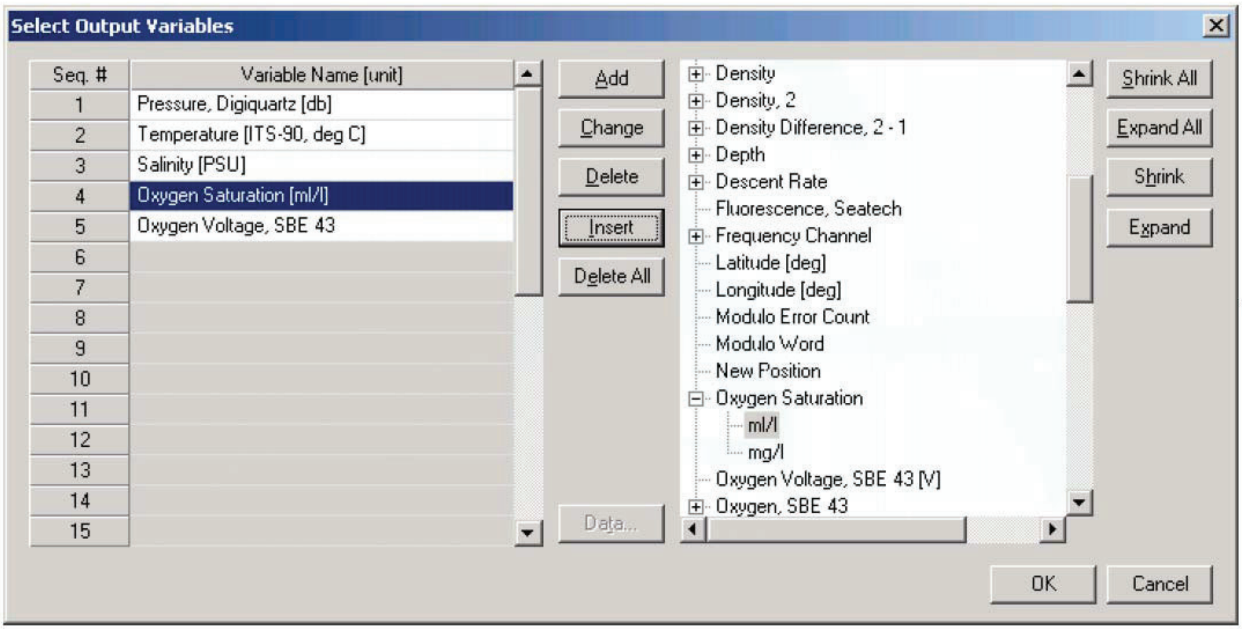

After selecting all the variables, click *OK* to return to the Data Conversion Data Setup tab. Then click *Start Process* to create the *.ros* file.

For this example, the *.ros* file contains 10 seconds of data centered on the moment the bottle closure occurred for every bottle closure. To make a useful table, select Rosette Summary from SBE Data Processing's Run menu. Rosette Summary calculates averages and standard deviations for the variables selected in Data Conversion. Select the appropriate *.con* and *.ros* files on the *File Setup* tab. Click the *Data Setup* tab and then click the *Select Averaged Variables* button; the dialog box is shown below.

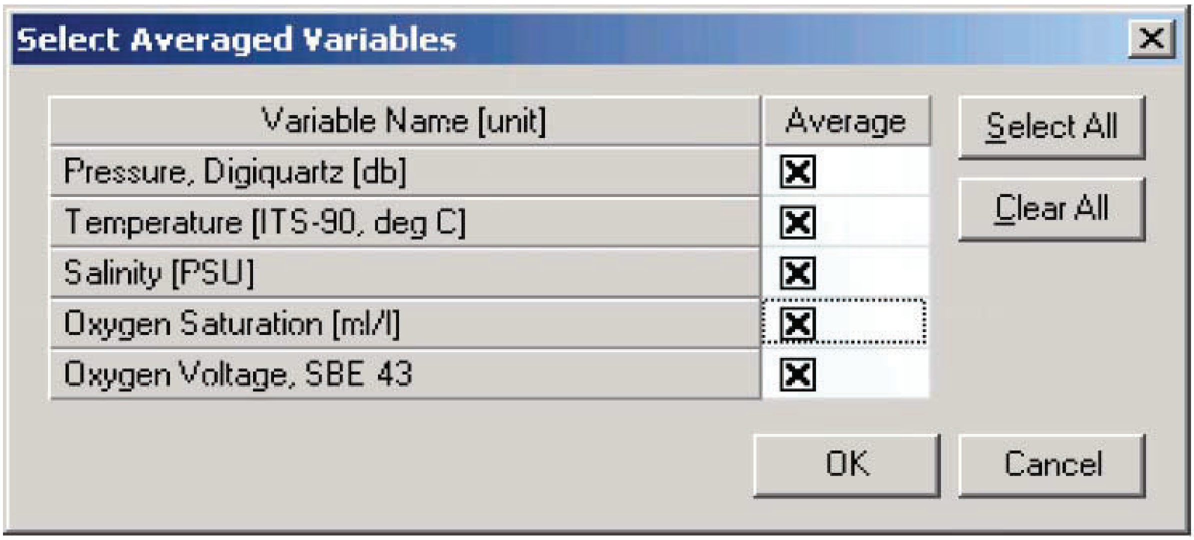

After selecting all the variables, click *OK* to return to the Rosette Summary Data Setup tab. Then click *Start Process* to create a data table file with the *.btl* extension.

Create a table with average pressure, temperature, salinity, oxygen saturation, and SBE 43 output voltage for each water sampler closure depth, by importing the *.btl* file into a spreadsheet. Then, enter by hand the Winkler titration dissolved oxygen values from your titration log, matching water sampler closures to pressures.

Calculate $\phi = Oxsol(T,S) * \left(1.0 + A*T + B*T^2 + C*T^3\right) * e^{\left(\frac{E*P}{K}\right)}$,

using *A, B, C,* and *E* from the SBE 43 calibration sheet.
Then, calculate $Winkler\ O_2 / \phi$.

Perform a linear regression, with:

- $Winkler\ O_2 / \phi$ (shown as Winkler/phi in the table) as the *Y* data
- SBE 43 output voltages as the *X* data

If a spreadsheet or statistical calculator is not available, the regression equations are:

$$M = \frac{n * \sum\left(V * \frac{Winkler\, O_2}{\phi}\right) - \sum V * \sum\left(\frac{Winkler\, O_2}{\phi}\right)}{n * \sum V^2 - \left(\sum V\right)^2}$$

$$B = \frac{\sum\left(\frac{Winkler\, O_2}{\phi}\right) - M * \sum V}{n}$$

Where:

n = number of data pairs
M = Slope
B = Offset

And:

$Soc = M$
$Voffset = B/M$

Reference

Owens, W. B., and R. C. Millard Jr., 1985: A new algorithm for CTD oxygen calibration. J. Phys. Oceanogr., 15, 621-631.
(NOTE: calibration expressed as ml/l)

3.2 Oxygen Bottle Samples

Oxygen samples were drawn first from every bottle. Duplicate samples were taken on each cast, usually from the first two bottles. Samples were drawn into clear, wide necked calibrated glass bottles and fixed on deck with reagents dispensed using Aquastep bottle top dispensers. A test station used to check on the oxygen bottle calibrations and as an opportunity to train a number of people to take the samples. The samples were shaken on deck and again in the laboratory 1/2 hour after collection, when the bottles were checked for the tightness of the stoppers and presence of bubbles. The samples were then stored under water until analysis.

Bottle temperatures were taken, following sampling for oxygen, using a hand held electronic thermometer probe. The temperatures were used to calculate any temperature-dependent changes in the sample bottle volumes.

Samples were analyzed in the constant temperature laboratory, starting three hours after sample collection, following the Winkler whole bottle titration with an amperometric method of endpoint detection, as described by Culberson (1991). The equipment used was supplied by Metrohm and included the Titrino unit and control pad, exchange unit with 10 ml burette to dispense the thiosulphate in increments of $2\ \mu l$, with an electrode for amperometric end point detection.
The difference for the duplicate pairs sampled on each station was in a range 0.00-0.02 ml/l.

The thiosulphate normality was checked on each run and recalculated every time the reservoir was topped up against potassium iodate. The exact weight of this standard, the calibrated 5 ml exchange unit driven by a Metrohm Dosimat and the 1L glass volumetric flask used to dispense and prepare the standard.

The introduction of oxygen with the reagents and impurities in the manganese chloride were corrected for by blank measurements made on each run, as described in the WOCE Manual of Operations and Methods (Culberson, 1991).

Collected data shows that dissolved oxygen concentrations varied from 4,71 to 8,06 ml/l. In order to control the accuracy of the oxygen measurements at each cast were taken parallel samples from the 1-2 bottles or duplicate samples.

Reproducibility of measurements

1953 samples were taken during the cruise; in addition 41 duplicates were analyzed. These include both duplicates taken from the same bottle (replicates) and those taken from different bottles fired at the same depth. The data gave a standard deviation of 0.007 ml/l.

3.3 Nutrient Bottle Samples

Samples for nutrient measurements were collected following oxygen samples from each Niskin bottle. Water was collected in clean plastic containers that had been rinsed three times by seawater through the latex tube.

Concentrations of silicate and phosphate were determined by photometric methods with spectrophotometer Shimadzu UVmini-1240. All samples were analyzed immediately after sampling.

Silicate determined by Korolev's method based on colorimeter of blue silicomolybdic complex (methodology described in Modern methods..., 1992). The ascorbic acid used as a restorative. The absorbance was read at 810 nm. Relative error of this method on concentration of dissolved silicate at 4.5 μM is ±4%, on concentration at 45 μM - ± 2,5%. Measured concentrations were in a range from 0.20 to 20.71 μM.

Phosphates determined according to the method Murphy and Raily (Modern methods..., 1992). Phosphate, dissolved in sea water, react with ammonium molibdate in a presence of sulfuric acid and tartrate potassium-antimony. The generated complex aggregate of phosphomolybdic heteropolyacid and trivalent antimony restorative by the ascorbic acid, and then determined the absorbance at 885 nm (we use the cavity 10cm). Relative error of this method ± 1%.

In order to ensure accuracy and increase precision of determination 3-5 duplicate samples were analyzed at each run. The mean difference for the duplicate pairs sampled on each station was in an error limit of the methods.

References:

Culberson, C.H. 1991.15 pp in the WOCE Operations Manual (WHP Operations and Methods) WHPO 91/1, Woods Hole.

Modern methods of hydrochemical research of the ocean, 1992. IO RAS, Moscow (in Russian).

3.4 Lowered Acoustic Doppler Current Profiler (LADCP)

The TRDI WHS 300 kHz ADCPs consists of a pressure case rated to 6000 meters with 4 transducers at one end in a convex arrangement and the beams diverging at 20 degrees from the vertical. At the opposite end to the transducers is a connector that enables downloading of data and connects it to other pressure cases containing another ADCP and the power supply pack. This arrangement allowed the ADCPs and the battery pack to be mounted vertically as up and down-looking on the CTD frame. Connection amongst all units was established using star cable with three male and two female terminations. Two male cable ends were always attached to the frame, this enabled comms leads to be readily connected pre and post deployment.

Communications: The 25-m communication leads (which also allow external power to be supplied to the ADCP) were sufficiently long to route it through to the port side of the deck lab where it was connected to a dedicated PC and external power supply. The latter was set at 48+ volts and was left on whilst the ADCP was on deck. 5 minutes prior to deployment the external power supply was shut off, the instrument checked and the configuration file sent to the ADCP as described in the manual instructions. The free end of the fly leads was greased and the end cap refitted, this was then taped to the frame for security.

Post deployment: When the CTD/LADCP was brought inboard, the fly-lead connectors were dried and the comms leads were connected to them. This stopped undue bending of the cables and kept them clear of the water bottles, aiding sampling. External power was applied again and the cast data downloaded as per the manual with a baud rate of 57600. The processing is accomplished using software developed by Visbeck after transferring the data to the PC.

Battery power was supplied to the ADCP in the form of 42 volts from 28 x 1.5 volt alkaline cells. Four of these packs were available for the cruise, as the ADCP will function at a minimum of 32 volts this was deemed an adequate stock for the duration.

Data quality: The data quality from the ADCP was good throughout. Due to the bad weather instrument titles sometimes exceeded 12° and this data was rejected during processing.

The LADCPs seem to function well and generates useful information on currents. The battery supply has its limitations though and thought should be given to alternatives to the present set-up.

3.4.1 LADCP Processing for Current Profiles

A brief account of the LADCP current data processing, file nomenclature and directory structure is provided in the following lines. Little emphasis is put into a detailed description of the main programming tools used, since these are part of a standard software package developed by Gerd Krahmann (version 10.13).

Outline of LADCP current calculation method

The Broad Band LADCP used during AMK77 cruise was designed to measure the instantaneous relative velocities of scatterers in the water column by taking advantage of the Doppler frequency shift, phase changes and correlation between coded pulses transmitted and received by the LADCP's four transducers. Conversion of this raw data stream to a profile of absolute currents involved an elaborate calculation method.

Firstly, Doppler shifts needed to be scaled to velocity units by taking into account the depth-dependent sound velocity (estimated from CTD T and S measurements). Directions could be inferred from trigonometric calculations based on the geometry of the transducer set, the orientation of the package (measured with a flux gate compass) and the local magnetic declination. The depth of the instrument was calculated from the integration of the measured vertical velocity and later adjusted to match the depth given by the CTD's pressure sensor.

The velocities corresponding to each single ensemble (or, in effect, to each transducer ping) were gridded in bins of depth set 8 meters. Statistical rejection of spiky measurements within each of these bins followed.

In order to reject the unwanted motion of the instrument (but also the barotropic component of the current), shear profiles were calculated for each ensemble. A complicated editing scheme preceded this shear calculation. A final shear profile (baroclinic current) was derived by real- depth gridding of the shear profiles calculated for individual ensembles. It was hoped that any relative velocities introduced by the high-frequency motion of the CTD package would be smoothed out by this repeated averaging.

The barotropic component of the flow was finally calculated from bottom-tracking measurements (bottom-track mode) or, in most occasions, in an integral sense from differential GPS positions of the ship (water-track mode).

The definitive velocity profile was hence obtained as the sum of the baroclinic and barotropic components.

During AMK77 cruise, no specific error calculation was performed. Profiles of shear standard deviation were included in the cast log sheet folder. Internal wave signals were obvious throughout the cruise.

Relevant PC files

The raw data were downloaded from the LADCP into a devoted PC after each cast and stored as a binary file called vNNNNm_01.000 for Master and vNNNNs_01.000 for Slave the c:\ladcp\AMK77\dNNN directory, where NNNN stands for the CTD cast number, e.g. raw data from cast 6333 were stored in the files d:\AMK77\data\ladcp\v6333m_01.000 and v5657s_01..000.

The configuration files (named Mconf.txt and Sconf.txt) containing the operating instructions (setting of track mode, bin depth, etc.) given to the LADCP previously to deployment was stored in the same directory.

Text files of the form NNNNm.log and NNNNs.log are the log of the 'bbtalk' session (testing the state and functioning of the instrument) previous to deployment. The details of the sessions for every single cast in the cruise are to be found in the cast log sheets.

A whole variety of files were created and manipulated during the different processing stages, and no mention will be made of the majority of them for reasons of clarity. The processing procedure may be summarised in two steps:

1- create CTD pressure, temperature and salinity data file as well as navigation collected every second in order to obtain the best possible estimates of depth and sound velocity. This is done using 'SBE Data Processing software and ConvLADCP Fortran program.

2- use the Gerd Krahmann's standard matlab package (v.10.13) with P. Lherminier's improvements (LPO, IFREMER) to process LADCP and CTD data

References

M. Visbeck 2002 Deep Velocity Profiling using Lowered Acoustic Doppler Current Profiler: Bottom Track and Inverse Solutions J. Atmos. Oceanic Technol. 10, 764-773.

3.5 Geological studies in the North Atlantic

The goal of this study was to describe the modern sediment system of the North Atlantic and to collect cores for a high-resolution reconstruction of climate change.

The research team had several objectives: an atmospheric aerosol study; collection of water samples to estimate the concentration and composition of suspended matter, including total and organic carbon, and phytoplankton pigments; collection of bottom sediment samples; microbiological and biogeochemical studies; and recovery and deployment of mooring stations (MS).

Atmospheric aerosols. A TSI AeroTrak APC-9303-01 airborne particle counter, (United States) was used to obtain the granulometric spectrum of aerosol particles in the surface layer. The atmospheric suspended particulate matter in surface layer was sampled using nylon nets.

Suspended sediment matter. The water was sampled for suspended sediment studies at the surface along the ship's route and in the ocean interior at oceanographic stations. To estimate the total concentration of the suspended matter, seawater was filtered under a vacuum of –0.4 atm through preliminary weighted nuclear filters 47 mm in diameter (pore diameter of 0.45 μm). To find the concentration of suspended organic carbon and chlorophyll, filtration was done through preliminarily calcinated Whatman GF/F glass fiber filters with a diameter of 47 mm (effective pore size of approximately 0.7 μm) under a vacuum of –0.2 atm in order to remove organic substances. The filters for the total content of the suspended particulate matter were dried in situ, and the glass fiber filters for the calculation of chlorophyll content were frozen and transported in a container with silicagel to Moscow. The content of suspended organic carbon was calculated on an AN-7529 device at the Institute of Oceanology, Russian Academy of Sciences. The concentrations of phytoplankton pigments (chlorophyll a and pheophytin a) were determined by the fluorometric method using a Turner Trilogy fluorimeter, which was preliminarily gauged at the Chair of Biophysics of the Department of Biology, Moscow State University. The contents of Si, Al, and P were estimated by the photometric method.

Bottom sediments. Large samples of bottom sediments were extracted with an Okean-0.25 Grab Sampler (GS), and sediment cores were recovered with a Multicorer 71.500 KC Denmark (MC) and a Gravity Corer (GC). Five cores from the GC, 19 minicores with above-bottom water from the MC and 27 minicores from the GS were carried out in total. Mineral composition of the sediments was examined with the help of microscope POLAM L-213M, foraminifera composition was examined with the help of binocular Bresser Advance ICD. Iceberg-rafted debris (IRD) was studied too.

Microbiological studies. At key stations of the studied transect, a set of measurements was carried out to assess the activity of microbial carbon and serum transformation, including the intensity of microbial carbon dioxide assimilation and methanogenesis and sulfidogenesis efficiency. Some samples were collected to define the isotopic composition of organic and mineral carbon in the suspended matter and bottom sediment. An express analysis was performed to assess the oxidation–reduction potential of sediment and the alkaline reserve of pore water.

Preliminary results

Prevailing wind directions were northwest, and northeast during the entire transit along the transect. The granulometric spectrum of surface layer aerosols varies depending on the wind state. The highest concentration of the aerosols in the underwater layer (40000 particles per L) was found in the North and Baltic Seas.

Suspended matter concentrations were found to be in a range from 0.07 to 1.4 mg/L. The highest concentrations were observed rather close to the coast (the North Sea and Greenland), but also in areas affected by the Irminger and North Atlantic currents. As for the vertical profiles, the highest concentrations were marked out in the upper ocean mixed layer (to a depth of 50 m), and for most of cases, at the surface (0 m). At nearly all stations, an increase in suspended matter concentration was found in the near-bottom layer. The highest concentrations (40–500 mg/L) were found in the above-bottom water from the MC samples.

The upper sediment layer consisted mainly of carbon silt-pelite sediments, with sandy dimension foraminipheric debris and material of ice rafting. The pattern of active bioturbation was noted at every station.

3.6 Carbonate system measurements

Grupo QUIMA. Instituto de Oceanografía y Cambio Global. Universidad de Las Palmas de Gran Canaria. 35017 Las Palmas de Gran Canaria. Spain

The QUIMA-ULPGC group has been invited by Drs. Gladyshev and Sokov from Shirshov Institute of Oceanology (SIO), Russian Academy of Science to collaborate in the project “Interannual monitoring of thermohaline and current structure along 59.5º N for evaluation of climate change in the North Atlantic” inside the hydrographic section 59.30N (A1E) and in the section of Denmark Strait, as responsible of the carbon parameters measurements. Studies related with Fe(II) kinetics in different water masses in the Irminger sea have also been included.

The research developed by the QUIMA group has been financed by the Project ATOPFe (CTM2017-83476-P) (Effects of ocean acidification, temperature and organic matter on Fe(II) persistence in the Atlantic Ocean) by the Ministerio de Economía y Competitividad from Spain.

The ATOPFe Project, in the objective 1.1, focuses on the effects of pH and T in the oxidation kinetics of Fe(II) in the A1E (59.5ºN) hydrographic section, in the area of Irminger sea, in order to compare these studies with experiments undertaken in the lab and to develop a kinetic model for iron in the context of ocean acidification.

Three members of the group participated in the cruise, Dr. Melchor González-Dávila, Dr. J. Magdalena Santana-Casiano and the technician Adrián Castro-Álamo. The data treatment and discussions of the results are responsibility of Dr. J. M. Santana-Casiano and Dr. Melchor González-Dávila

From 8-8-2019 to 8-9-2019 the Oceanography Cruise AMK77 took place on board R/V *Akademik Mstislav Keldysh* departing from Arkhangelsk Harbor. Two sections were done.

- The first (section 1), the section 59.5ºN, from Scotland to Greenland
- The second (section 2) between Greenland-Iceland in the Denmark Strait.

Measured parameters

In both sections two parameters of the carbon dioxide system were measured along the water column in order to achieve the highest level of data quality and resolution:

- The total alkalinity, A_T in µmol kg^{-1} was measured by potentiometer (Mintrop et al., 2000).

- The total dissolved inorganic carbon, C_T in µmol kg^{-1}, was measured using a VINDTA 3C system by coulometry (Mintrop et al., 2000, González-Dávila et al., 2003).

- Certified Reference Material, CRMs, acquired to Dr. Andrew Dickson at Scripps Institution of Oceanography, San Diego, California, were used each day after a new cell was prepared, both for A_T and C_T variables. Therefore, the values for the two variables were accurate to ± 1.5 µmol kg^{-1} for A_T and ± 1.0 µmol kg^{-1} for C_T. Reproducibility of the CRMs analyzed during the cruise was better than ± 1.0 µmol kg^{-1} for both variables.

- In order to do a consistency exercise between the measured variables and the best set of constants for the calculation of the carbonate system parameters, UV-Vis spectrophotometric pH measurements were also done in selected stations.

In the Irminger Sea, samples for Fe(II) kinetics studies and samples for TOC (Total organic carbon) were taken and frozen.

Sampling procedure

For the CO_2 system studies 500 ml glass bottles were used for the determination of both A_T and C_T. The bottles were rinsed twice with seawater and over-filled with seawater from the bottom. Samples were preserved from light and analysed between stations. CRMs (batch 177) were used for the A_T and C_T quality control.

For the Fe(II) studies 250 ml LDPE bottles washed according GEOTRACES protocols were used. 50 ml LDPE bottles were also sampled at each depth in order to provide Total Organic Carbon, TOC (Santana-González et al., 2018, 2019). The studies will be carried out in the QUIMA-ULPGC lab (Santana-Casiano et al., 2005).

Stations and parameters sampled

CO_2 system

For the study of the CO_2 system, stations 6283 to 6331 (section 1) and 6332 to 6445 (section 2) were sampled. Table 1 shows the number of stations sampled for each section and the amount of samples measured for A_T and C_T and pH. A total of 152 stations have been done considering both sections, with 1962 Niskin bottles closed (replicated bottles for biology studies have not been considered) and 1594 Niskin sampled for the carbon dioxide parameters. 93 samples were analyzed for UV-Vis spectrophotometric pH for the consistency exercise, 1594 for total alkalinity and 1594 for total dissolved inorganic carbon.

Fe(II) kinetics studies

For Fe(II) studies, the stations in section 1, those from 6320 to 6330 were sampled with a total of 100 samples for Fe(II) kinetics studies and 72 for TOC.

	Stations	N Niskin	N sample	pH	A_T	C_T
SECTION 1	48	952	831	20	831	831
SECTION2	104	1010	763	73	763	763
TOTAL	152	1962	1594	93	1594	1594

Table 1. Total number of analyzed samples for pH, Total alkalinity (A_T) and Total dissolved inorganic carbon (C_T) during the cruise AMK77 by the QUIMA-ULPGC group.

References

1. Mintrop, L., Pérez, F.F., González-Dávila, M., Santana-Casiano, J.M., Körtzinger, A., 2000. Alkalinity determination by potentiometry: Intercalibration using three different methods, Ciencias Marinas 26, 23-37.
2. González-Dávila, M., Santana-Casiano, J. M., Rueda, M. J., Llinás, O., González-Dávila, E., 2003. Seasonal and interanual variability of sea-surface carbon dioxide species at the European station for Time Series in the Ocean at the Canary Islands (ESTOC) between 1996 and 2000. Global. Biochem. Cycles 17(3), 1076, doi:10.1029/2002GB001993.
3. Santana-Casiano, J. M., González-Dávila, M., Millero, F. J. 2005. Oxidation of nanomolar level of Fe(II) with oxygen in natural waters. Environ. Sci. Technol. 39, 2073-2079
4. Santana-González, C., Santana-Casiano, J. M., González-Dávila, M., Santana-del-Pino, A., Gladyshev, S., Sokov, A., 2018. Fe(II) oxidation kinetics in the North Atlantic along the 59.5° N during 2016. Marine Chemistry., 203, 64-77.

5. Santana-González, C., González-Dávila, M., Santana-Casiano, J. M., Gladyshev, S., Sokov, A., 2019. Organic matter effect on Fe(II) oxidation kinetics in the Labrador Sea. Chem. Geol., 511, 238-255.

.　CRUISE LOGISTICS

Mobilization

Mobilization for the cruise took place on the way from Arkhangelsk (Russia) to the first station of the cruise. It took seven days. The scientific team arrived at the ship on August 07^{th}.

ACKNOWLEDGEMENTS

The principal scientists would like to thank the Master, officers, crew and scientists of the RV *Akademik Mstislav Keldysh* for making this such an enjoyable, as well as successful cruise.

TABLES

FIGURES

Fig. l Station locations in AMK77 cruise.

Fig.2 Vertical distribution of samples along the 59.5 section.

Fig. 3. Schematic diagram of the large-scale circulation in the northern North Atlantic compiled from [Schmitz and McCartney, 1993; Schott and Brandt, 2007; Sutherland and Pickart, 2008; Lherminier et al., 2010]. Abbreviations for the main topographic features, currents and water masses are explained in the legend. The nominal locations of the 59.5°N hydrographic section (1997 – present) and sections across the straits between Greenland, Iceland, Faeroe and Shetland Islands (2011 – present) are shown with the solid green lines.

Fig. 4. Oxygen concentrations (ml/l) in the water column (lower panel) as observed in March–October 1997 in four hydrographic sections (upper panel) ending nearby the southern tip of Greenland. A separate oxygen maximum in the LSW layer (1000–2000 m) in the Irminger Sea at 59.5°N strongly implies local convective renewal of LSW before 1997. Adapted from [Falina et al., 2007].

Fig. 5. Warming and salinification in the northern North Atlantic between the mid-1990s and mid-2000s, as observed at 59.5°N. The figure shows the 2006–1997 temperature (°C, left) and salinity (right) differences on isobaric surfaces in the Irminger Sea and Iceland Basin. Adapted from [Sarafanov et al., 2007].

Fig. 6. Coherence of the decadal salinity changes (1950s – 2000s) of the intermediate (LSW) and deep (ISOW) waters in the northern North Atlantic and their link to the North Atlantic Oscillation (NAO) index. **(a)** Schematic representation of the LSW and ISOW pathways and locations of the Icelandic Low (L) and Azores High (H) centers constituting the NAO dipole pattern. The red dotted line indicates the 59.5°N transatlantic section. **(b)** Salinity time series for LSW in the Labrador Sea [Yashayaev, 2007] and ISOW in the Iceland basin [Boessenkool et al., 2007; Sarafanov et al., 2007] overlaid by the third order polynomial fits. **(c)** Time series of the winter NAO index, after [Hurrell, 1995], overlaid by 7-year running mean and third order polynomial fit. **(d)** Mechanism of the NAO effect on the decadal changes in temperature (T) and salinity (S) of the northern North Atlantic intermediate and deep waters. Positive / negative links shown with the dark / light grey arrows mean that changes in 'causative' and 'consequential' characteristics have the same / opposite sign(s). The overall effect of the NAO on T and S of the in the water column is negative: persistent NAO decline leads to warming and salinification of the water masses and vice versa, as shown in (b) and (c). Adapted from [Sarafanov, 2009].

Fig. 7. Schematic representation of the upper-ocean circulation and convection intensity in the northern North Atlantic under high (left) and low (right) NAO conditions. Blue (magenta) solid

arrows indicate the upper-ocean flows with higher fraction of colder fresher subpolar (warmer saltier subtropical) waters. The main pathways of the Nordic overflow-derived deep waters are shown with the dotted curves. "C" and "E" symbols are used to denote, respectively, the deep convection sites and the domain, where the Atlantic waters are entrained into ISOW. Larger (smaller) circles indicate stronger (weaker) convection. SPG and STG – the subpolar and subtropical gyres, respectively. Adapted from [Sarafanov, 2009].

Fig. 8. The Deep Western Boundary Current (DWBC) transport variability and its link to the convection intensity in the Labrador Sea. **(a)** Locations of the hydrographic sections (1991–2007) and schematic of the deep water circulation in the Irminger Sea. **(b)** The DWBC transport anomalies at Cape Farewell in 1991–2007, 1 Sv = 10^6 m^3 s^{-1}. The 1994–1997 and 2000–2007 mean anomalies and the 1994–2007 linear trend are shown. **(c)** Anomalies of the DWBC transport at Cape Farewell and the Labrador Sea Water (LSW) thickness in the Labrador Sea in the 1950s–2000s. **(d)** Correlation coefficient (R^2) for the two times series shown in **(c)** at the 0–5-year lag, the LSW thickness leads. The correlation maximum is achieved at the 1–3-year lag. The DWBC transport anomalies in the southern Irminger Sea are foregone by the convection intensity anomalies in the Labrador Sea. Adapted from [Sarafanov et al., 2009].

Fig. 9. Schematic diagram of the Meridional Overturning Circulation (MOC) at the northern periphery of the Atlantic Ocean, northeast of Cape Farewell. The dotted lines refer to the σ_0 isopycnals 27.55 and 27.80. The arrows denote the integral meridional and diapycnal volume fluxes. Where the signs are specified, the positive (negative) transports are northward (southward). The NAC and EGIC transports in the upper layer ($\sigma_0 < 27.55$) at 59.5°N are the throughputs accounting for the recirculations. EGIC – the East Greenland / Irminger Current – refers to the upper part of the Western Boundary Current. Other abbreviations are explained in the legend to **Fig. 3**. Adapted from [Sarafanov et al., 2012].

Fig. 10. Salinity observed in the northwestern Irminger Sea at 64.3°N in February 1998. The σ_0 isopycnals 27.55, 27.70, 27.80 and 27.88 are plotted as the thick black lines; the station locations are marked with the ticks on the top axis. The plot shows fresh dense waters descending (cascading) down the continental slope of Greenland down to the LSW layer ($27.70 < \sigma_0 < 27.80$) and the layer of the Nordic Seas overflow-derived deep waters ($\sigma_0 > 27.80$). Adapted from [Falina et al., 2012].

Fig. 11. One-hour averaged atmospheric pressure (mb) measured during the 59.5 section 77 cruise of *Akademik Mstislav Keldysh*.

Fig. 12. One-hour air temperature (°C) measured during the 59.5 section 77 cruise of *Akademik Mstislav Keldysh*.

Fig. 13 Regression lines for Winkler oxygen divided by φ versus SBE 43 output voltage for (a) and (b) 59.5 transatlantic section, (c) the DS Experiment II.

Fig. 14 The vertical distribution of (a) potential temperature (°C), (b) salinity (PSU) and (c) dissolved oxygen (μmol/kg) along 59.5 N in 15-24 August 2019. Potential density is shown in white. Station position is shown by vertical marks.

Table 1

R/V AK. MSTISLAV KELDYSH CRUISE 77

Sta	Date	Time	Pos	Lat	Lon	Depth	Above Bottom	Bottles	Measurements
6283	081619	0712	BE	59 30.0 N	004 36.0 W	88	1	8	CTD,LADCP,Chemistry
6283	081619	0723	BO	59 30.0 N	004 35.9 W	88	1	8	CTD,LADCP,Chemistry
6283	081619	0736	EN	59 30.0 N	004 35.8 W	88	1	8	CTD,LADCP,Chemistry
6284	081619	1006	BE	59 30.0 N	005 17.9 W	109	4	19	CTD,LADCP,Chemistry
6284	081619	1013	BO	59 30.1 N	005 17.7 W	109	4	19	CTD,LADCP,Chemistry
6284	081619	1026	EN	59 30.2 N	005 17.4 W	109	4	19	CTD,LADCP,Chemistry
6285	081619	1245	BE	59 30.1 N	006 00.2 W	136	4	8	CTD,LADCP,Chemistry
6285	081619	1258	BO	59 30.0 N	006 00.0 W	136	4	8	CTD,LADCP,Chemistry
6285	081619	1310	EN	59 30.1 N	006 00.0 W	136	4	8	CTD,LADCP,Chemistry
6286	081619	1527	BE	59 30.2 N	006 39.7 W	570	6	13	CTD,LADCP,Chemistry
6286	081619	1547	BO	59 30.0 N	006 39.9 W	570	6	13	CTD,LADCP,Chemistry
6286	081619	1611	EN	59 30.0 N	006 39.9 W	570	6	13	CTD,LADCP,Chemistry
6287	081619	1840	BE	59 30.1 N	007 20.0 W	1056	7	21	CTD,LADCP,Chemistry
6287	081619	1907	BO	59 30.0 N	007 19.7 W	1056	7	21	CTD,LADCP,Chemistry
6287	081619	1948	EN	59 29.9 N	007 20.4 W	1056	7	21	CTD,LADCP,Chemistry
6288	081619	2207	BE	59 30.0 N	008 00.0 W	1143	9	21	CTD,LADCP,Chemistry
6288	081619	2232	BO	59 30.0 N	007 59.4 W	1143	9	21	CTD,LADCP,Chemistry
6288	081619	2322	EN	59 30.1 N	007 58.5 W	1143	9	21	CTD,LADCP,Chemistry
6289	081719	0142	BE	59 30.1 N	008 39.8 W	1364	8	20	CTD,LADCP,Chemistry
6289	081719	0214	BO	59 30.0 N	008 39.8 W	1364	8	20	CTD,LADCP,Chemistry
6289	081719	0313	EN	59 29.9 N	008 39.4 W	1364	8	20	CTD,LADCP,Chemistry
6290	081719	0530	BE	59 30.1 N	009 19.7 W	1487	10	19	CTD,LADCP,Chemistry
6290	081719	0606	BO	59 30.0 N	009 20.0 W	1487	10	19	CTD,LADCP,Chemistry
6290	081719	0645	EN	59 30.0 N	009 20.1 W	1487	10	19	CTD,LADCP,Chemistry
6291	081719	0905	BE	59 29.9 N	009 59.9 W	1049	6	21	CTD,LADCP,Chemistry
6291	081719	0932	BO	59 30.2 N	009 59.3 W	1049	6	21	CTD,LADCP,Chemistry
6291	081719	1000	EN	59 30.4 N	009 58.7 W	1049	6	21	CTD,LADCP,Chemistry
6291g	081719	1023	BE	59 30.0 N	009 59.6 W	1049	-99	19	CTD,LADCP,Chemistry
6291g	081719	1031	BO	59 30.0 N	009 59.6 W	1049	-99	19	CTD,LADCP,Chemistry
6291g	081719	1040	EN	59 30.0 N	009 59.5 W	1049	-99	19	CTD,LADCP,Chemistry
6292	081719	1258	BE	59 30.1 N	010 40.0 W	1523	5	20	CTD,LADCP,Chemistry
6292	081719	1330	BO	59 29.9 N	010 40.3 W	1523	5	20	CTD,LADCP,Chemistry
6292	081719	1412	EN	59 29.7 N	010 40.8 W	1523	5	20	CTD,LADCP,Chemistry

6293	081719	1624	BE	59 30.0 N	011 20.0 W	1611	4	20	CTD,LADCP,Chemistry
6293	081719	1701	BO	59 29.9 N	011 20.3 W	1611	4	20	CTD,LADCP,Chemistry
6293	081719	1751	EN	59 30.1 N	011 20.6 W	1611	4	20	CTD,LADCP,Chemistry
6294	081719	1959	BE	59 30.0 N	012 00.0 W	1504	9	21	CTD,LADCP,Chemistry
6294	081719	2029	BO	59 30.1 N	012 00.4 W	1504	9	21	CTD,LADCP,Chemistry
6294	081719	2112	EN	59 30.3 N	012 00.5 W	1504	9	21	CTD,LADCP,Chemistry
6295	081719	2316	BE	59 29.9 N	012 40.0 W	1361	10	21	CTD,LADCP,Chemistry
6295	081719	2347	BO	59 30.0 N	012 40.1 W	1361	10	21	CTD,LADCP,Chemistry
6295	081819	0046	EN	59 29.8 N	012 40.8 W	1361	10	21	CTD,LADCP,Chemistry
6296	081819	0253	BE	59 29.8 N	013 19.9 W	1307	6	21	CTD,LADCP,Chemistry
6296	081819	0325	BO	59 29.8 N	013 20.1 W	1307	6	21	CTD,LADCP,Chemistry
6296	081819	0423	EN	59 29.5 N	013 20.4 W	1307	6	21	CTD,LADCP,Chemistry
6297	081819	0632	BE	59 29.8 N	013 59.9 W	997	6	16	CTD,LADCP,Chemistry
6297	081819	0659	BO	59 29.9 N	014 00.0 W	997	6	16	CTD,LADCP,Chemistry
6297	081819	0729	EN	59 29.9 N	014 00.1 W	997	6	16	CTD,LADCP,Chemistry
6298	081819	0941	BE	59 29.8 N	014 39.8 W	988	2	19	CTD,LADCP,Chemistry
6298	081819	1005	BO	59 29.8 N	014 40.1 W	988	2	19	CTD,LADCP,Chemistry
6298	081819	1031	EN	59 29.9 N	014 40.1 W	988	2	19	CTD,LADCP,Chemistry
6298g	081819	1052	BE	59 30.0 N	014 39.7 W	988	-99	20	CTD,LADCP,Chemistry
6298g	081819	1059	BO	59 30.0 N	014 39.8 W	988	-99	20	CTD,LADCP,Chemistry
6298g	081819	1109	EN	59 30.0 N	014 39.8 W	988	-99	20	CTD,LADCP,Chemistry
6299	081819	1322	BE	59 29.7 N	015 19.4 W	1525	7	19	CTD,LADCP,Chemistry
6299	081819	1359	BO	59 29.7 N	015 20.0 W	1525	7	19	CTD,LADCP,Chemistry
6299	081819	1439	EN	59 29.4 N	015 20.0 W	1525	7	19	CTD,LADCP,Chemistry
6300	081819	1658	BE	59 29.9 N	015 59.9 W	1536	7	19	CTD,LADCP,Chemistry
6300	081819	1730	BO	59 29.8 N	016 00.0 W	1536	7	19	CTD,LADCP,Chemistry
6300	081819	1813	EN	59 29.9 N	015 59.9 W	1536	7	19	CTD,LADCP,Chemistry
6301	081819	2028	BE	59 30.0 N	016 39.9 W	1103	4	19	CTD,LADCP,Chemistry
6301	081819	2052	BO	59 30.0 N	016 39.8 W	1103	4	19	CTD,LADCP,Chemistry
6301	081819	2127	EN	59 30.1 N	016 39.8 W	1103	4	19	CTD,LADCP,Chemistry
6302	081819	2350	BE	59 29.8 N	017 19.7 W	1753	4	21	CTD,LADCP,Chemistry
6302	081919	0027	BO	59 29.7 N	017 19.9 W	1753	4	21	CTD,LADCP,Chemistry
6302	081919	0128	EN	59 29.5 N	017 19.7 W	1753	4	21	CTD,LADCP,Chemistry
6303	081919	0346	BE	59 29.9 N	017 59.7 W	2184	3	21	CTD,LADCP,Chemistry
6303	081919	0429	BO	59 30.0 N	017 59.9 W	2184	3	21	CTD,LADCP,Chemistry
6303	081919	0538	EN	59 30.0 N	018 00.0 W	2184	3	21	CTD,LADCP,Chemistry

6304	081919	0756	BE	59 29.9 N	018 39.8 W	2735	4	21	CTD,LADCP,Chemistry
6304	081919	0848	BO	59 29.9 N	018 39.9 W	2735	4	21	CTD,LADCP,Chemistry
6304	081919	0946	EN	59 29.8 N	018 40.0 W	2735	4	21	CTD,LADCP,Chemistry
6304g	081919	1013	BE	59 29.9 N	018 39.9 W	2735	-99	18	CTD,LADCP,Chemistry
6304g	081919	1021	BO	59 29.9 N	018 40.0 W	2735	-99	18	CTD,LADCP,Chemistry
6304g	081919	1031	EN	59 29.9 N	018 40.1 W	2735	-99	18	CTD,LADCP,Chemistry
6305	081919	1244	BE	59 29.9 N	019 19.7 W	2743	3	21	CTD,LADCP,Chemistry
6305	081919	1336	BO	59 29.8 N	019 20.0 W	2743	3	21	CTD,LADCP,Chemistry
6305	081919	1437	EN	59 30.0 N	019 19.8 W	2743	3	21	CTD,LADCP,Chemistry
6306	081919	1653	BE	59 29.9 N	019 59.6 W	2809	9	21	CTD,LADCP,Chemistry
6306	081919	1749	BO	59 30.0 N	019 59.6 W	2809	9	21	CTD,LADCP,Chemistry
6306	081919	1853	EN	59 30.0 N	019 59.5 W	2809	9	21	CTD,LADCP,Chemistry
6307	081919	2108	BE	59 29.8 N	020 40.0 W	2823	5	21	CTD,LADCP,Chemistry
6307	081919	2200	BO	59 29.6 N	020 40.2 W	2823	5	21	CTD,LADCP,Chemistry
6307	081919	2316	EN	59 29.6 N	020 40.6 W	2823	5	21	CTD,LADCP,Chemistry
6308	082019	0112	BE	59 30.0 N	021 19.8 W	2899	6	21	CTD,LADCP,Chemistry
6308	082019	0314	BO	59 30.5 N	021 19.5 W	2899	6	21	CTD,LADCP,Chemistry
6308	082019	0333	EN	59 30.7 N	021 19.4 W	2899	6	21	CTD,LADCP,Chemistry
6309	082019	1449	BE	59 30.0 N	021 59.9 W	2787	5	20	CTD,LADCP,Chemistry
6309	082019	1540	BO	59 30.2 N	021 59.4 W	2787	5	20	CTD,LADCP,Chemistry
6309	082019	1645	EN	59 30.2 N	021 59.4 W	2787	5	20	CTD,LADCP,Chemistry
6309g	082019	1055	BE	59 30.0 N	022 00.2 W	2787	-99		CTD,LADCP
6309g	082019	1124	BO	59 30.0 N	022 00.0 W	2787	-99		CTD,LADCP
6309g	082019	1124	EN	59 30.0 N	022 00.0 W	2787	-99		CTD,LADCP
6310	082019	1902	BE	59 30.0 N	022 39.9 W	2503	10	21	CTD,LADCP,Chemistry
6310	082019	1949	BO	59 30.0 N	022 39.0 W	2503	10	21	CTD,LADCP,Chemistry
6310	082019	2051	EN	59 30.1 N	022 37.8 W	2503	10	21	CTD,LADCP,Chemistry
6311	082119	0008	BO	59 30.0 N	023 20.0 W	2438	8	21	CTD,LADCP,Chemistry
6311	082119	0122	EN	59 30.2 N	023 19.6 W	2438	8	21	CTD,LADCP,Chemistry
6311	082019	2325	BE	59 30.0 N	023 20.1 W	2438	8	21	CTD,LADCP,Chemistry
6312	082119	0334	BE	59 29.9 N	023 59.7 W	2565	9	21	CTD,LADCP,Chemistry
6312	082119	0425	BO	59 30.0 N	023 59.9 W	2565	9	21	CTD,LADCP,Chemistry
6312	082119	0537	EN	59 29.8 N	024 00.1 W	2565	9	21	CTD,LADCP,Chemistry
6313	082119	0755	BE	59 29.9 N	024 39.7 W	2569	9	20	CTD,LADCP,Chemistry
6313	082119	0845	BO	59 29.7 N	024 39.9 W	2569	9	20	CTD,LADCP,Chemistry
6313	082119	0936	EN	59 29.7 N	024 40.0 W	2569	9	20	CTD,LADCP,Chemistry

6313g	082119	1002	BE	59 30.0 N	024 40.2 W	2569	-99	21	CTD,LADCP,Chemistry
6313g	082119	1012	BO	59 30.0 N	024 40.3 W	2569	-99	21	CTD,LADCP,Chemistry
6313g	082119	1023	EN	59 30.0 N	024 40.4 W	2569	-99	21	CTD,LADCP,Chemistry
6314	082119	1237	BE	59 30.0 N	025 19.9 W	2496	7	21	CTD,LADCP,Chemistry
6314	082119	1325	BO	59 29.9 N	025 19.6 W	2496	7	21	CTD,LADCP,Chemistry
6314	082119	1424	EN	59 29.8 N	025 19.7 W	2496	7	21	CTD,LADCP,Chemistry
6315	082119	1647	BE	59 29.9 N	025 59.9 W	2300	4	21	CTD,LADCP,Chemistry
6315	082119	1733	BO	59 29.8 N	026 00.1 W	2300	4	21	CTD,LADCP,Chemistry
6315	082119	1829	EN	59 29.8 N	026 00.3 W	2300	4	21	CTD,LADCP,Chemistry
6316	082119	2042	BE	59 29.9 N	026 39.9 W	2236	4	21	CTD,LADCP,Chemistry
6316	082119	2128	BO	59 29.8 N	026 40.5 W	2236	4	21	CTD,LADCP,Chemistry
6316	082119	2234	EN	59 29.6 N	026 41.4 W	2236	4	21	CTD,LADCP,Chemistry
6317	082219	0035	BE	59 29.8 N	027 19.9 W	1913	2	21	CTD,LADCP,Chemistry
6317	082219	0118	BO	59 29.8 N	027 20.1 W	1913	2	21	CTD,LADCP,Chemistry
6317	082219	0223	EN	59 29.7 N	027 19.6 W	1913	2	21	CTD,LADCP,Chemistry
6318	082219	0440	BE	59 29.8 N	027 59.9 W	2004	3	21	CTD,LADCP,Chemistry
6318	082219	0521	BO	59 29.9 N	028 00.1 W	2004	3	21	CTD,LADCP,Chemistry
6318	082219	0617	EN	59 30.0 N	028 00.2 W	2004	3	21	CTD,LADCP,Chemistry
6319	082219	0826	BE	59 29.9 N	028 40.0 W	1683	1	21	CTD,LADCP,Chemistry
6319	082219	0901	BO	59 29.9 N	028 40.6 W	1683	1	21	CTD,LADCP,Chemistry
6319	082219	0942	EN	59 30.0 N	028 41.2 W	1683	1	21	CTD,LADCP,Chemistry
6319g	082219	1009	BE	59 29.9 N	028 41.1 W	1683	-99	21	CTD,LADCP,Chemistry
6319g	082219	1015	BO	59 29.9 N	028 41.1 W	1683	-99	21	CTD,LADCP,Chemistry
6319g	082219	1026	EN	59 29.9 N	028 41.1 W	1683	-99	21	CTD,LADCP,Chemistry
6320	082219	1225	BE	59 29.8 N	029 20.1 W	1431	8	20	CTD,LADCP,Chemistry
6320	082219	1258	BO	59 29.8 N	029 20.4 W	1431	8	20	CTD,LADCP,Chemistry
6320	082219	1337	EN	59 29.7 N	029 21.0 W	1431	8	20	CTD,LADCP,Chemistry
6321	082219	1645	BE	59 29.8 N	030 00.0 W	1488	5	20	CTD,LADCP,Chemistry
6321	082219	1721	BO	59 30.0 N	030 00.0 W	1488	5	20	CTD,LADCP,Chemistry
6321	082219	1804	EN	59 30.0 N	029 59.9 W	1488	5	20	CTD,LADCP,Chemistry
6322	082219	2011	BE	59 29.9 N	030 39.9 W	1528	5	20	CTD,LADCP,Chemistry
6322	082219	2042	BO	59 30.0 N	030 39.9 W	1528	5	20	CTD,LADCP,Chemistry
6322	082219	2128	EN	59 30.0 N	030 39.9 W	1528	5	20	CTD,LADCP,Chemistry
6323	082219	2340	BE	59 29.9 N	031 19.8 W	1701	2	21	CTD,LADCP,Chemistry
6323	082319	0017	BO	59 30.2 N	031 20.5 W	1701	2	21	CTD,LADCP,Chemistry
6323	082319	0117	EN	59 30.2 N	031 20.5 W	1701	2	21	CTD,LADCP,Chemistry

6324	082319	0332	BE	59 29.8 N	031 59.9 W	1941	10	21	CTD,LADCP,Chemistry
6324	082319	0413	BO	59 29.9 N	032 00.1 W	1941	10	21	CTD,LADCP,Chemistry
6324	082319	0515	EN	59 29.9 N	032 00.6 W	1941	10	21	CTD,LADCP,Chemistry
6325	082319	0721	BE	59 29.9 N	032 39.6 W	2039	9	21	CTD,LADCP,Chemistry
6325	082319	0804	BO	59 29.6 N	032 39.7 W	2039	9	21	CTD,LADCP,Chemistry
6325	082319	0850	EN	59 29.2 N	032 39.8 W	2039	9	21	CTD,LADCP,Chemistry
6325g	082319	0917	BE	59 29.9 N	032 40.1 W	2039	-99	21	CTD,LADCP,Chemistry
6325g	082319	0926	BO	59 29.8 N	032 40.1 W	2039	-99	21	CTD,LADCP,Chemistry
6325g	082319	0939	EN	59 29.7 N	032 40.1 W	2039	-99	21	CTD,LADCP,Chemistry
6326	082319	1149	BE	59 29.9 N	033 19.9 W	2217	2	21	CTD,LADCP,Chemistry
6326	082319	1233	BO	59 30.0 N	033 19.8 W	2217	2	21	CTD,LADCP,Chemistry
6326	082319	1324	EN	59 30.1 N	033 19.8 W	2217	2	21	CTD,LADCP,Chemistry
6327	082319	1550	BE	59 29.9 N	033 59.8 W	2513	5	21	CTD,LADCP,Chemistry
6327	082319	1639	BO	59 30.0 N	033 59.9 W	2513	5	21	CTD,LADCP,Chemistry
6327	082319	1742	EN	59 30.0 N	034 00.0 W	2513	5	21	CTD,LADCP,Chemistry
6328	082319	2219	BE	59 29.9 N	034 39.7 W	2711	5	21	CTD,LADCP,Chemistry
6328	082319	2309	BO	59 29.9 N	034 39.7 W	2711	5	21	CTD,LADCP,Chemistry
6328	082419	0024	EN	59 29.8 N	034 39.7 W	2711	5	21	CTD,LADCP,Chemistry
6328a	082319	1945	BE	59 29.9 N	034 39.2 W	2831	4	1	CTD,LADCP,Chemistry
6328a	082319	2045	BO	59 29.9 N	034 39.9 W	2831	4	1	CTD,LADCP,Chemistry
6328a	082319	2048	EN	59 29.9 N	034 39.9 W	2831	4	1	CTD,LADCP,Chemistry
6329	082419	0201	BE	59 29.9 N	035 09.7 W	3106	3	21	CTD,LADCP,Chemistry
6329	082419	0300	BO	59 29.9 N	035 09.9 W	3106	3	21	CTD,LADCP,Chemistry
6329	082419	0423	EN	59 29.7 N	035 10.2 W	3106	3	21	CTD,LADCP,Chemistry
6330	082419	1012	BE	59 30.0 N	035 59.9 W	3093	4	20	CTD,LADCP,Chemistry
6330	082419	1110	BO	59 29.9 N	035 59.8 W	3093	4	20	CTD,LADCP,Chemistry
6330	082419	1215	EN	59 30.1 N	035 59.5 W	3093	4	20	CTD,LADCP,Chemistry
6330g	082419	1238	BE	59 30.1 N	035 59.4 W	250	99	20	CTD,LADCP,Chemistry
6330g	082419	1245	BO	59 30.1 N	035 59.4 W	250	99	20	CTD,LADCP,Chemistry
6330g	082419	1253	EN	59 30.1 N	035 59.4 W	250	99	20	CTD,LADCP,Chemistry
6331	082419	1432	BE	59 30.1 N	036 25.5 W	2776	6	21	CTD,LADCP,Chemistry
6331	082419	1524	BO	59 30.1 N	036 25.4 W	2776	6	21	CTD,LADCP,Chemistry
6331	082419	1627	EN	59 30.4 N	036 25.0 W	2776	6	21	CTD,LADCP,Chemistry
6332	082719	1155	BE	66 19.9 N	028 08.2 W	343	4	15	CTD,LADCP,Chemistry
6332	082719	1207	BO	66 19.9 N	028 08.5 W	343	4	15	CTD,LADCP,Chemistry
6332	082719	1224	EN	66 19.8 N	028 09.0 W	343	4	15	CTD,LADCP,Chemistry

6333	082719	1315	BE	66 23.1 N	028 22.9 W	315	4	9	CTD,LADCP,Chemistry
6333	082719	1327	BO	66 23.1 N	028 22.9 W	315	4	9	CTD,LADCP,Chemistry
6333	082719	1339	EN	66 23.1 N	028 23.1 W	315	4	9	CTD,LADCP,Chemistry
6334	082719	1555	BE	66 14.4 N	027 46.2 W	470	4	10	CTD,LADCP,Chemistry
6334	082719	1614	BO	66 14.6 N	027 46.2 W	470	4	10	CTD,LADCP,Chemistry
6334	082719	1630	EN	66 14.7 N	027 46.5 W	470	4	10	CTD,LADCP,Chemistry
6335	082719	1732	BE	66 11.0 N	027 31.4 W	486	5	10	CTD,LADCP,Chemistry
6335	082719	1746	BO	66 11.1 N	027 31.7 W	486	5	10	CTD,LADCP,Chemistry
6335	082719	1802	EN	66 11.2 N	027 32.1 W	486	5	10	CTD,LADCP,Chemistry
6336	082719	1900	BE	66 07.7 N	027 17.7 W	529	2	10	CTD,LADCP,Chemistry
6336	082719	1916	BO	66 07.8 N	027 18.0 W	529	2	10	CTD,LADCP,Chemistry
6336	082719	1932	EN	66 07.8 N	027 18.4 W	529	2	10	CTD,LADCP,Chemistry
6337	082719	2024	BE	66 04.6 N	027 05.1 W	656	5	21	CTD,LADCP,Chemistry
6337	082719	2040	BO	66 04.5 N	027 05.5 W	656	5	21	CTD,LADCP,Chemistry
6337	082719	2058	EN	66 04.4 N	027 06.1 W	656	5	21	CTD,LADCP,Chemistry
6338	082719	2155	BE	66 00.7 N	026 49.1 W	446	4	16	CTD,LADCP,Chemistry
6338	082719	2212	BO	66 00.6 N	026 48.8 W	446	4	16	CTD,LADCP,Chemistry
6338	082719	2243	EN	66 00.6 N	026 48.8 W	446	4	16	CTD,LADCP,Chemistry
6339	082719	2352	BE	65 56.0 N	026 29.3 W	286	3	9	CTD,LADCP,Chemistry
6339	082819	0006	BO	65 55.9 N	026 28.8 W	286	3	9	CTD,LADCP,Chemistry
6339	082819	0024	EN	65 55.9 N	026 28.8 W	286	3	9	CTD,LADCP,Chemistry
6340	082819	0158	BE	65 49.7 N	026 00.2 W	225	3	8	CTD,LADCP,Chemistry
6340	082819	0211	BO	65 49.7 N	026 00.0 W	225	3	8	CTD,LADCP,Chemistry
6340	082819	0231	EN	65 49.5 N	026 00.3 W	225	3	8	CTD,LADCP,Chemistry
6341	082819	0348	BE	65 44.8 N	025 38.7 W	276	3	9	CTD,LADCP,Chemistry
6341	082819	0405	BO	65 44.8 N	025 38.7 W	276	3	9	CTD,LADCP,Chemistry
6341	082819	0422	EN	65 44.8 N	025 38.8 W	276	3	9	CTD,LADCP,Chemistry
6342	082819	0704	BE	65 55.9 N	026 29.1 W	291	4	9	CTD,LADCP,Chemistry
6342	082819	0717	BO	65 56.1 N	026 29.1 W	291	4	9	CTD,LADCP,Chemistry
6342	082819	0729	EN	65 56.3 N	026 29.0 W	291	4	9	CTD,LADCP,Chemistry
6343	082819	0842	BE	66 00.6 N	026 48.9 W	450	3	21	CTD,LADCP,Chemistry
6343	082819	0855	BO	66 00.6 N	026 48.7 W	450	3	21	CTD,LADCP,Chemistry
6343	082819	0912	EN	66 00.6 N	026 48.3 W	450	3	21	CTD,LADCP,Chemistry
6344	082819	1009	BE	66 04.5 N	027 04.8 W	666	8	18	CTD,LADCP,Chemistry
6344	082819	1028	BO	66 04.3 N	027 05.2 W	666	8	18	CTD,LADCP,Chemistry
6344	082819	1052	EN	66 03.7 N	027 05.7 W	666	8	18	CTD,LADCP,Chemistry

6345	082819	1144	BE	66 07.8 N	027 18.3 W	528	4	10	CTD,LADCP,Chemistry
6345	082819	1157	BO	66 07.6 N	027 18.6 W	528	4	10	CTD,LADCP,Chemistry
6345	082819	1213	EN	66 07.4 N	027 18.9 W	528	4	10	CTD,LADCP,Chemistry
6346	082819	1305	BE	66 11.0 N	027 31.7 W	485	5	9	CTD,LADCP,Chemistry
6346	082819	1319	BO	66 10.8 N	027 31.6 W	485	5	9	CTD,LADCP,Chemistry
6346	082819	1334	EN	66 10.6 N	027 31.7 W	485	5	9	CTD,LADCP,Chemistry
6347	082819	1430	BE	66 14.7 N	027 45.6 W	470	2	10	CTD,LADCP,Chemistry
6347	082819	1446	BO	66 14.8 N	027 45.1 W	470	2	10	CTD,LADCP,Chemistry
6347	082819	1501	EN	66 14.7 N	027 45.1 W	470	2	10	CTD,LADCP,Chemistry
6348	082819	1616	BE	66 19.7 N	028 07.8 W	344	5	8	CTD,LADCP,Chemistry
6348	082819	1632	BO	66 20.0 N	028 08.2 W	344	5	8	CTD,LADCP,Chemistry
6348	082819	1645	EN	66 20.0 N	028 08.1 W	344	5	8	CTD,LADCP,Chemistry
6349	082819	1758	BE	66 14.8 N	027 45.4 W	473	5	9	CTD,LADCP,Chemistry
6349	082819	1811	BO	66 14.7 N	027 45.1 W	473	5	9	CTD,LADCP,Chemistry
6349	082819	1827	EN	66 14.6 N	027 45.0 W	473	5	9	CTD,LADCP,Chemistry
6350	082819	1914	BE	66 11.0 N	027 31.6 W	485	2	14	CTD,LADCP,Chemistry
6350	082819	1929	BO	66 10.9 N	027 31.6 W	485	2	14	CTD,LADCP,Chemistry
6350	082819	1950	EN	66 10.8 N	027 31.3 W	485	2	14	CTD,LADCP,Chemistry
6351	082819	2032	BE	66 07.8 N	027 18.2 W	544	6	11	CTD,LADCP,Chemistry
6351	082819	2034	BO	66 07.7 N	027 18.0 W	544	6	11	CTD,LADCP,Chemistry
6351	082819	2107	EN	66 07.4 N	027 18.3 W	544	6	11	CTD,LADCP,Chemistry
6352	082819	2150	BE	66 04.6 N	027 05.1 W	658	3	13	CTD,LADCP,Chemistry
6352	082819	2206	BO	66 04.3 N	027 05.4 W	658	3	13	CTD,LADCP,Chemistry
6352	082819	2235	EN	66 03.8 N	027 06.1 W	658	3	13	CTD,LADCP,Chemistry
6353	082819	2329	BE	66 00.6 N	026 49.2 W	446	2	10	CTD,LADCP,Chemistry
6353	082819	2346	BO	66 00.5 N	026 49.1 W	446	2	10	CTD,LADCP,Chemistry
6353	082919	0010	EN	66 00.4 N	026 49.4 W	446	2	10	CTD,LADCP,Chemistry
6354	082919	0121	BE	65 55.8 N	026 29.3 W	284	5	8	CTD,LADCP,Chemistry
6354	082919	0128	BO	65 55.9 N	026 29.1 W	284	5	8	CTD,LADCP,Chemistry
6354	082919	0151	EN	65 55.9 N	026 29.4 W	284	5	8	CTD,LADCP,Chemistry
6355	082919	0257	BE	66 00.5 N	026 48.9 W	457	4	12	CTD,LADCP,Chemistry
6355	082919	0303	BO	66 00.6 N	026 49.0 W	457	4	12	CTD,LADCP,Chemistry
6355	082919	0339	EN	66 00.6 N	026 50.0 W	457	4	12	CTD,LADCP,Chemistry
6356	082919	0429	BE	66 04.4 N	027 04.6 W	661	5	15	CTD,LADCP,Chemistry
6356	082919	0446	BO	66 04.4 N	027 05.5 W	661	5	15	CTD,LADCP,Chemistry
6356	082919	0523	EN	66 03.9 N	027 06.3 W	661	5	15	CTD,LADCP,Chemistry

6357	082919	0614	BE	66 07.9 N	027 17.8 W	530	5	10	CTD,LADCP,Chemistry
6357	082919	0621	BO	66 07.9 N	027 17.8 W	530	5	10	CTD,LADCP,Chemistry
6357	082919	0644	EN	66 07.9 N	027 18.0 W	530	5	10	CTD,LADCP,Chemistry
6358	082919	0906	BE	66 11.0 N	027 31.5 W	485	4	10	CTD,LADCP,Chemistry
6358	082919	0917	BO	66 11.0 N	027 31.4 W	485	4	10	CTD,LADCP,Chemistry
6358	082919	0933	EN	66 11.0 N	027 31.3 W	485	4	10	CTD,LADCP,Chemistry
6359	082919	1028	BE	66 14.8 N	027 45.4 W	471	4	15	CTD,LADCP,Chemistry
6359	082919	1041	BO	66 14.8 N	027 45.4 W	471	4	15	CTD,LADCP,Chemistry
6359	082919	1059	EN	66 14.7 N	027 45.3 W	471	4	15	CTD,LADCP,Chemistry
6360	082919	1214	BE	66 19.8 N	028 08.4 W	343	6	21	CTD,LADCP,Chemistry
6360	082919	1227	BO	66 19.9 N	028 08.4 W	343	6	21	CTD,LADCP,Chemistry
6360	082919	1241	EN	66 19.7 N	028 08.6 W	343	6	21	CTD,LADCP,Chemistry
6361	082919	1356	BE	66 14.8 N	027 45.4 W	474	5	10	CTD,LADCP,Chemistry
6361	082919	1411	BO	66 14.7 N	027 45.5 W	474	5	10	CTD,LADCP,Chemistry
6361	082919	1428	EN	66 14.6 N	027 45.9 W	474	5	10	CTD,LADCP,Chemistry
6362	082919	1518	BE	66 11.0 N	027 31.6 W	485	3	21	CTD,LADCP,Chemistry
6362	082919	1533	BO	66 10.9 N	027 31.7 W	485	3	21	CTD,LADCP,Chemistry
6362	082919	1548	EN	66 10.8 N	027 32.0 W	485	3	21	CTD,LADCP,Chemistry
6363	082919	1636	BE	66 07.8 N	027 18.3 W	527	4	12	CTD,LADCP,Chemistry
6363	082919	1653	BO	66 07.8 N	027 18.2 W	527	4	12	CTD,LADCP,Chemistry
6363	082919	1711	EN	66 07.9 N	027 18.7 W	527	4	12	CTD,LADCP,Chemistry
6364	082919	1758	BE	66 04.8 N	027 05.1 W	656	6	21	CTD,LADCP,Chemistry
6364	082919	1817	BO	66 04.7 N	027 05.4 W	656	6	21	CTD,LADCP,Chemistry
6364	082919	1837	EN	66 04.5 N	027 06.2 W	656	6	21	CTD,LADCP,Chemistry
6365	082919	1908	BE	66 02.9 N	026 57.3 W	597	4		CTD,LADCP
6365	082919	1929	BO	66 03.0 N	026 56.9 W	597	4		CTD,LADCP
6365	082919	1940	EN	66 03.1 N	026 57.1 W	597	4		CTD,LADCP
6366	082919	2012	BE	66 00.7 N	026 49.3 W	460	6	10	CTD,LADCP,Chemistry
6366	082919	2032	BO	66 01.1 N	026 48.5 W	460	6	10	CTD,LADCP,Chemistry
6366	082919	2046	EN	66 01.6 N	026 48.3 W	460	6	10	CTD,LADCP,Chemistry
6367	082919	2202	BE	65 55.9 N	026 29.3 W	289	2	21	CTD,LADCP,Chemistry
6367	082919	2218	BO	65 56.0 N	026 29.0 W	289	2	21	CTD,LADCP,Chemistry
6367	082919	2238	EN	65 56.2 N	026 29.0 W	289	2	21	CTD,LADCP,Chemistry
6368	082919	2342	BE	66 00.5 N	026 48.8 W	458	4	12	CTD,LADCP,Chemistry
6368	082919	2358	BO	66 00.8 N	026 48.9 W	458	4	12	CTD,LADCP,Chemistry
6368	083019	0023	EN	66 01.2 N	026 48.5 W	458	4	12	CTD,LADCP,Chemistry

6369	083019	0117	BE	66 04.5 N	027 05.0 W	654	4	14	CTD,LADCP,Chemistry
6369	083019	0137	BO	66 04.4 N	027 05.7 W	654	4	14	CTD,LADCP,Chemistry
6369	083019	0208	EN	66 03.9 N	027 07.4 W	654	4	14	CTD,LADCP,Chemistry
6370	083019	0234	BE	66 06.1 N	027 11.6 W	621	5		CTD,LADCP
6370	083019	0254	BO	66 06.0 N	027 12.4 W	621	5		CTD,LADCP
6370	083019	0306	EN	66 05.8 N	027 13.2 W	621	5		CTD,LADCP
6371	083019	0330	BE	66 07.7 N	027 18.1 W	523	5	14	CTD,LADCP,Chemistry
6371	083019	0346	BO	66 07.7 N	027 18.8 W	523	5	14	CTD,LADCP,Chemistry
6371	083019	0417	EN	66 07.4 N	027 20.2 W	523	5	14	CTD,LADCP,Chemistry
6372	083019	0501	BE	66 11.0 N	027 31.3 W	486	3	12	CTD,LADCP,Chemistry
6372	083019	0516	BO	66 11.0 N	027 31.8 W	486	3	12	CTD,LADCP,Chemistry
6372	083019	0543	EN	66 10.7 N	027 32.4 W	486	3	12	CTD,LADCP,Chemistry
6373	083019	0754	BE	66 08.4 N	026 50.7 W	651	4	11	CTD,LADCP,Chemistry
6373	083019	0813	BO	66 08.8 N	026 51.0 W	651	4	11	CTD,LADCP,Chemistry
6373	083019	0832	EN	66 09.2 N	026 51.2 W	651	4	11	CTD,LADCP,Chemistry
6374	083019	0926	BE	66 12.2 N	026 36.1 W	613	2	14	CTD,LADCP,Chemistry
6374	083019	0941	BO	66 12.3 N	026 36.2 W	613	2	14	CTD,LADCP,Chemistry
6374	083019	1002	EN	66 12.4 N	026 36.5 W	613	2	14	CTD,LADCP,Chemistry
6375	083019	1102	BE	66 16.0 N	026 21.4 W	592	5	21	CTD,LADCP,Chemistry
6375	083019	1117	BO	66 15.9 N	026 21.5 W	592	5	21	CTD,LADCP,Chemistry
6375	083019	1136	EN	66 15.8 N	026 21.7 W	592	5	21	CTD,LADCP,Chemistry
6376	083019	1236	BE	66 19.8 N	026 06.7 W	588	3	9	CTD,LADCP,Chemistry
6376	083019	1251	BO	66 19.7 N	026 07.0 W	588	3	9	CTD,LADCP,Chemistry
6376	083019	1308	EN	66 19.5 N	026 07.4 W	588	3	9	CTD,LADCP,Chemistry
6377	083019	1404	BE	66 12.8 N	026 17.2 W	537	5	9	CTD,LADCP,Chemistry
6377	083019	1422	BO	66 12.8 N	026 17.4 W	537	5	9	CTD,LADCP,Chemistry
6377	083019	1440	EN	66 12.7 N	026 17.7 W	537	5	9	CTD,LADCP,Chemistry
6378	083019	1610	BE	66 12.2 N	026 50.1 W	622	3	9	CTD,LADCP,Chemistry
6378	083019	1625	BO	66 12.1 N	026 50.6 W	622	3	9	CTD,LADCP,Chemistry
6378	083019	1642	EN	66 11.9 N	026 51.5 W	622	3	9	CTD,LADCP,Chemistry
6379	083019	1740	BE	66 04.8 N	027 04.3 W	654	5	14	CTD,LADCP,Chemistry
6379	083019	1801	BO	66 04.8 N	027 06.0 W	654	5	14	CTD,LADCP,Chemistry
6379	083019	1822	EN	66 04.9 N	027 07.2 W	654	5	14	CTD,LADCP,Chemistry
6380	083019	1948	BE	65 56.8 N	027 34.5 W	612	4	9	CTD,LADCP,Chemistry
6380	083019	2008	BO	65 56.8 N	027 34.9 W	612	4	9	CTD,LADCP,Chemistry
6380	083019	2025	EN	65 56.7 N	027 35.1 W	612	4	9	CTD,LADCP,Chemistry

6381	083019	2048	BE	65 55.3 N	027 41.2 W	617	5		CTD,LADCP
6381	083019	2104	BO	65 55.3 N	027 41.2 W	617	5		CTD,LADCP
6381	083019	2116	EN	65 55.2 N	027 41.4 W	617	5		CTD,LADCP
6382	083019	2138	BE	65 53.7 N	027 47.1 W	627	6		CTD,LADCP
6382	083019	2155	BO	65 53.7 N	027 47.2 W	627	6		CTD,LADCP
6382	083019	2207	EN	65 53.6 N	027 47.1 W	627	6		CTD,LADCP
6383	083019	2242	BE	65 51.2 N	027 57.7 W	664	4		CTD,LADCP
6383	083019	2302	BO	65 51.1 N	027 57.8 W	664	4		CTD,LADCP
6383	083019	2315	EN	65 51.0 N	027 57.9 W	664	4		CTD,LADCP
6384	083019	2349	BE	65 48.6 N	028 08.3 W	715	5		CTD,LADCP
6384	083119	0008	BO	65 48.5 N	028 08.7 W	715	5		CTD,LADCP
6384	083119	0022	EN	65 48.4 N	028 08.7 W	715	5		CTD,LADCP
6385	083119	0244	BE	65 58.8 N	027 26.8 W	621	4		CTD,LADCP
6385	083119	0305	BO	65 58.9 N	027 27.1 W	621	4		CTD,LADCP
6385	083119	0317	EN	65 58.9 N	027 27.5 W	621	4		CTD,LADCP
6386	083119	0357	BE	66 01.3 N	027 17.0 W	630	4		CTD,LADCP
6386	083119	0417	BO	66 01.4 N	027 18.1 W	630	4		CTD,LADCP
6386	083119	0429	EN	66 01.4 N	027 18.9 W	630	4		CTD,LADCP
6387	083119	0655	BE	65 55.9 N	026 29.2 W	290	5	9	CTD,LADCP,Chemistry
6387	083119	0705	BO	65 56.0 N	026 29.1 W	290	5	9	CTD,LADCP,Chemistry
6387	083119	0716	EN	65 56.0 N	026 28.9 W	290	5	9	CTD,LADCP,Chemistry
6388	083119	0824	BE	66 00.5 N	026 48.6 W	456	4	14	CTD,LADCP,Chemistry
6388	083119	0839	BO	66 00.8 N	026 48.5 W	456	4	14	CTD,LADCP,Chemistry
6388	083119	0856	EN	66 01.1 N	026 48.0 W	456	4	14	CTD,LADCP,Chemistry
6389	083119	0949	BE	66 04.7 N	027 04.9 W	654	5	12	CTD,LADCP,Chemistry
6389	083119	1004	BO	66 04.9 N	027 05.3 W	654	5	12	CTD,LADCP,Chemistry
6389	083119	1024	EN	66 05.1 N	027 05.8 W	654	5	12	CTD,LADCP,Chemistry
6390	083119	1104	BE	66 07.8 N	027 18.1 W	521	5	21	CTD,LADCP,Chemistry
6390	083119	1118	BO	66 07.9 N	027 18.5 W	521	5	21	CTD,LADCP,Chemistry
6390	083119	1135	EN	66 07.9 N	027 19.1 W	521	5	21	CTD,LADCP,Chemistry
6391	083119	1217	BE	66 11.0 N	027 31.5 W	484	4	9	CTD,LADCP,Chemistry
6391	083119	1231	BO	66 11.1 N	027 31.6 W	484	4	9	CTD,LADCP,Chemistry
6391	083119	1246	EN	66 11.0 N	027 31.8 W	484	4	9	CTD,LADCP,Chemistry
6392	083119	1335	BE	66 14.8 N	027 45.3 W	471	4	21	CTD,LADCP,Chemistry
6392	083119	1348	BO	66 14.8 N	027 45.3 W	471	4	21	CTD,LADCP,Chemistry
6392	083119	1404	EN	66 14.7 N	027 45.4 W	471	4	21	CTD,LADCP,Chemistry

6393	083119	1513	BE	66 19.9 N	028 08.0 W	343	6	8	CTD,LADCP,Chemistry
6393	083119	1525	BO	66 19.9 N	028 08.3 W	343	6	8	CTD,LADCP,Chemistry
6393	083119	1538	EN	66 19.8 N	028 08.4 W	343	6	8	CTD,LADCP,Chemistry
6394	083119	1653	BE	66 14.9 N	027 45.6 W	477	4	10	CTD,LADCP,Chemistry
6394	083119	1708	BO	66 14.8 N	027 45.7 W	477	4	10	CTD,LADCP,Chemistry
6394	083119	1723	EN	66 14.8 N	027 45.9 W	477	4	10	CTD,LADCP,Chemistry
6395	083119	1811	BE	66 11.2 N	027 32.0 W	486	5	10	CTD,LADCP,Chemistry
6395	083119	1828	BO	66 11.1 N	027 31.8 W	486	5	10	CTD,LADCP,Chemistry
6395	083119	1845	EN	66 11.0 N	027 32.0 W	486	5	10	CTD,LADCP,Chemistry
6396	083119	1930	BE	66 07.9 N	027 18.8 W	520	3	10	CTD,LADCP,Chemistry
6396	083119	1948	BO	66 07.9 N	027 18.8 W	520	3	10	CTD,LADCP,Chemistry
6396	083119	2006	EN	66 08.0 N	027 19.2 W	520	3	10	CTD,LADCP,Chemistry
6397	083119	2050	BE	66 04.8 N	027 05.1 W	656	1	11	CTD,LADCP,Chemistry
6397	083119	2114	BO	66 05.0 N	027 04.5 W	656	1	11	CTD,LADCP,Chemistry
6397	083119	2138	EN	66 05.0 N	027 04.7 W	656	1	11	CTD,LADCP,Chemistry
6398	083119	2205	BE	66 02.8 N	026 57.1 W	595	5		CTD,LADCP
6398	083119	2222	BO	66 02.8 N	026 56.8 W	595	5		CTD,LADCP
6398	083119	2234	EN	66 02.9 N	026 56.5 W	595	5		CTD,LADCP
6399	083119	2301	BE	66 00.8 N	026 48.9 W	453	6	10	CTD,LADCP,Chemistry
6399	083119	2315	BO	66 00.7 N	026 48.4 W	453	6	10	CTD,LADCP,Chemistry
6399	083119	2338	EN	66 01.0 N	026 47.2 W	453	6	10	CTD,LADCP,Chemistry
6400	090119	0032	BE	65 56.0 N	026 29.3 W	286	4	8	CTD,LADCP,Chemistry
6400	090119	0045	BO	65 56.0 N	026 28.7 W	286	4	8	CTD,LADCP,Chemistry
6400	090119	0101	EN	65 56.0 N	026 28.5 W	286	4	8	CTD,LADCP,Chemistry
6401	090119	0211	BE	66 00.5 N	026 48.5 W	446	4	12	CTD,LADCP,Chemistry
6401	090119	0226	BO	66 00.5 N	026 48.5 W	446	4	12	CTD,LADCP,Chemistry
6401	090119	0250	EN	66 00.4 N	026 47.9 W	446	4	12	CTD,LADCP,Chemistry
6402	090119	0322	BE	66 02.6 N	026 56.6 W	586	5		CTD,LADCP
6402	090119	0340	BO	66 02.6 N	026 56.8 W	586	5		CTD,LADCP
6402	090119	0352	EN	66 02.5 N	026 56.6 W	586	5		CTD,LADCP
6403	090119	0424	BE	66 04.6 N	027 04.5 W	658	5	13	CTD,LADCP,Chemistry
6403	090119	0443	BO	66 04.5 N	027 04.9 W	658	5	13	CTD,LADCP,Chemistry
6403	090119	0512	EN	66 04.1 N	027 05.1 W	658	5	13	CTD,LADCP,Chemistry
6404	090119	0539	BE	66 06.2 N	027 11.2 W	620	4		CTD,LADCP
6404	090119	0556	BO	66 06.2 N	027 11.6 W	620	4		CTD,LADCP
6404	090119	0608	EN	66 06.0 N	027 11.9 W	620	4		CTD,LADCP

6405	090119	0637	BE	66 07.9 N	027 17.5 W	537	4	11	CTD,LADCP,Chemistry
6405	090119	0651	BO	66 07.7 N	027 17.6 W	537	4	11	CTD,LADCP,Chemistry
6405	090119	0707	EN	66 07.5 N	027 17.7 W	537	4	11	CTD,LADCP,Chemistry
6406	090119	0756	BE	66 11.0 N	027 31.1 W	486	5	15	CTD,LADCP,Chemistry
6406	090119	0810	BO	66 11.0 N	027 31.4 W	486	5	15	CTD,LADCP,Chemistry
6406	090119	0829	EN	66 10.9 N	027 31.2 W	486	5	15	CTD,LADCP,Chemistry
6407	090119	0921	BE	66 14.9 N	027 45.1 W	474	5	11	CTD,LADCP,Chemistry
6407	090119	0933	BO	66 14.9 N	027 44.9 W	474	5	11	CTD,LADCP,Chemistry
6407	090119	0949	EN	66 15.0 N	027 44.5 W	474	5	11	CTD,LADCP,Chemistry
6408	090119	1103	BE	66 20.0 N	028 07.9 W	343	5	8	CTD,LADCP,Chemistry
6408	090119	1115	BO	66 19.9 N	028 07.8 W	343	5	8	CTD,LADCP,Chemistry
6408	090119	1127	EN	66 19.9 N	028 07.4 W	343	5	8	CTD,LADCP,Chemistry
6409	090119	1231	BE	66 14.8 N	027 45.2 W	472	2	10	CTD,LADCP,Chemistry
6409	090119	1243	BO	66 14.9 N	027 44.8 W	472	2	10	CTD,LADCP,Chemistry
6409	090119	1258	EN	66 14.8 N	027 44.3 W	472	2	10	CTD,LADCP,Chemistry
6410	090119	1342	BE	66 11.2 N	027 31.4 W	484	5	10	CTD,LADCP,Chemistry
6410	090119	1356	BO	66 10.9 N	027 31.2 W	484	5	10	CTD,LADCP,Chemistry
6410	090119	1413	EN	66 10.7 N	027 30.7 W	484	5	10	CTD,LADCP,Chemistry
6411	090119	1453	BE	66 08.0 N	027 18.0 W	544	4	9	CTD,LADCP,Chemistry
6411	090119	1509	BO	66 07.5 N	027 17.7 W	544	4	9	CTD,LADCP,Chemistry
6411	090119	1526	EN	66 07.2 N	027 17.6 W	544	4	9	CTD,LADCP,Chemistry
6412	090119	1607	BE	66 04.7 N	027 05.4 W	655	6	14	CTD,LADCP,Chemistry
6412	090119	1624	BO	66 04.4 N	027 05.4 W	655	6	14	CTD,LADCP,Chemistry
6412	090119	1646	EN	66 04.1 N	027 05.7 W	655	6	14	CTD,LADCP,Chemistry
6413	090119	1713	BE	66 02.7 N	026 57.2 W	585	5		CTD,LADCP
6413	090119	1730	BO	66 02.6 N	026 56.8 W	585	5		CTD,LADCP
6413	090119	1741	EN	66 02.5 N	026 56.6 W	585	5		CTD,LADCP
6414	090119	1808	BE	66 00.7 N	026 49.4 W	453	4	8	CTD,LADCP,Chemistry
6414	090119	1824	BO	66 00.6 N	026 49.1 W	453	4	8	CTD,LADCP,Chemistry
6414	090119	1837	EN	66 00.7 N	026 48.8 W	453	4	8	CTD,LADCP,Chemistry
6415	090119	1941	BE	65 56.1 N	026 29.3 W	290	5	11	CTD,LADCP,Chemistry
6415	090119	1953	BO	65 56.0 N	026 29.1 W	290	5	11	CTD,LADCP,Chemistry
6415	090119	2007	EN	65 56.1 N	026 29.1 W	290	5	11	CTD,LADCP,Chemistry
6416	090119	2111	BE	66 00.7 N	026 48.7 W	455	4	9	CTD,LADCP,Chemistry
6416	090119	2122	BO	66 00.8 N	026 48.5 W	455	4	9	CTD,LADCP,Chemistry
6416	090119	2138	EN	66 01.1 N	026 48.3 W	455	4	9	CTD,LADCP,Chemistry

6417	090119	2230	BE	66 04.6 N	027 04.6 W	659	3	13	CTD,LADCP,Chemistry
6417	090119	2250	BO	66 04.7 N	027 05.0 W	659	3	13	CTD,LADCP,Chemistry
6417	090119	2320	EN	66 04.6 N	027 04.7 W	659	3	13	CTD,LADCP,Chemistry
6418	090119	2345	BE	66 06.3 N	027 11.2 W	613	5		CTD,LADCP
6418	090219	0002	BO	66 06.2 N	027 11.4 W	613	5		CTD,LADCP
6418	090219	0014	EN	66 06.1 N	027 11.2 W	613	5		CTD,LADCP
6419	090219	0042	BE	66 07.8 N	027 18.0 W	528	4	12	CTD,LADCP,Chemistry
6419	090219	0059	BO	66 07.8 N	027 18.0 W	528	4	12	CTD,LADCP,Chemistry
6419	090219	0126	EN	66 07.7 N	027 18.0 W	528	4	12	CTD,LADCP,Chemistry
6420	090219	0213	BE	66 11.2 N	027 31.4 W	484	5	12	CTD,LADCP,Chemistry
6420	090219	0229	BO	66 11.0 N	027 31.6 W	484	5	12	CTD,LADCP,Chemistry
6420	090219	0255	EN	66 11.0 N	027 31.7 W	484	5	12	CTD,LADCP,Chemistry
6421	090219	0347	BE	66 14.9 N	027 45.5 W	476	2	11	CTD,LADCP,Chemistry
6421	090219	0403	BO	66 14.8 N	027 45.9 W	476	2	11	CTD,LADCP,Chemistry
6421	090219	0428	EN	66 14.6 N	027 46.4 W	476	2	11	CTD,LADCP,Chemistry
6422	090219	0532	BE	66 19.9 N	028 07.9 W	344	5	10	CTD,LADCP,Chemistry
6422	090219	0547	BO	66 19.8 N	028 08.9 W	344	5	10	CTD,LADCP,Chemistry
6422	090219	0601	EN	66 19.7 N	028 09.6 W	344	5	10	CTD,LADCP,Chemistry
6423	090219	0724	BE	66 14.9 N	027 45.5 W	478	3	11	CTD,LADCP,Chemistry
6423	090219	0737	BO	66 14.8 N	027 45.9 W	478	3	11	CTD,LADCP,Chemistry
6423	090219	0752	EN	66 14.7 N	027 46.5 W	478	3	11	CTD,LADCP,Chemistry
6424	090219	0842	BE	66 11.2 N	027 31.8 W	486	5	10	CTD,LADCP,Chemistry
6424	090219	0857	BO	66 11.1 N	027 31.9 W	486	5	10	CTD,LADCP,Chemistry
6424	090219	0915	EN	66 11.1 N	027 31.8 W	486	5	10	CTD,LADCP,Chemistry
6425	090219	0958	BE	66 07.8 N	027 18.6 W	524	3	14	CTD,LADCP,Chemistry
6425	090219	1012	BO	66 07.7 N	027 18.6 W	524	3	14	CTD,LADCP,Chemistry
6425	090219	1033	EN	66 07.6 N	027 18.7 W	524	3	14	CTD,LADCP,Chemistry
6426	090219	1112	BE	66 04.8 N	027 05.4 W	658	5	15	CTD,LADCP,Chemistry
6426	090219	1131	BO	66 04.6 N	027 04.8 W	658	5	15	CTD,LADCP,Chemistry
6426	090219	1152	EN	66 04.5 N	027 04.4 W	658	5	15	CTD,LADCP,Chemistry
6427	090219	1215	BE	66 02.8 N	026 57.2 W	593	6		CTD,LADCP
6427	090219	1231	BO	66 02.9 N	026 56.5 W	593	6		CTD,LADCP
6427	090219	1243	EN	66 03.1 N	026 56.0 W	593	6		CTD,LADCP
6428	090219	1311	BE	66 00.7 N	026 49.0 W	452	4	8	CTD,LADCP,Chemistry
6428	090219	1324	BO	66 00.8 N	026 48.4 W	452	4	8	CTD,LADCP,Chemistry
6428	090219	1339	EN	66 01.1 N	026 47.9 W	452	4	8	CTD,LADCP,Chemistry

6429	090219	1436	BE	65 56.1 N	026 29.4 W	286	6	6	CTD,LADCP,Chemistry
6429	090219	1448	BO	65 55.9 N	026 28.9 W	286	6	6	CTD,LADCP,Chemistry
6429	090219	1459	EN	65 56.0 N	026 28.9 W	286	6	6	CTD,LADCP,Chemistry
6430	090219	1605	BE	66 00.4 N	026 48.4 W	447	1	9	CTD,LADCP,Chemistry
6430	090219	1621	BO	66 00.5 N	026 48.6 W	447	1	9	CTD,LADCP,Chemistry
6430	090219	1637	EN	66 00.7 N	026 48.4 W	447	1	9	CTD,LADCP,Chemistry
6431	090219	1706	BE	66 02.4 N	026 56.7 W	588	5		CTD,LADCP
6431	090219	1723	BO	66 02.6 N	026 56.9 W	588	5		CTD,LADCP
6431	090219	1734	EN	66 02.6 N	026 56.8 W	588	5		CTD,LADCP
6432	090219	1802	BE	66 04.5 N	027 04.9 W	654	5	10	CTD,LADCP,Chemistry
6432	090219	1819	BO	66 04.4 N	027 05.4 W	654	5	10	CTD,LADCP,Chemistry
6432	090219	1838	EN	66 04.3 N	027 06.2 W	654	5	10	CTD,LADCP,Chemistry
6433	090219	1859	BE	66 06.1 N	027 11.3 W	622	6		CTD,LADCP
6433	090219	1917	BO	66 06.0 N	027 12.2 W	622	6		CTD,LADCP
6433	090219	1929	EN	66 05.8 N	027 12.8 W	622	6		CTD,LADCP
6434	090219	1955	BE	66 07.9 N	027 18.2 W	520	5	8	CTD,LADCP,Chemistry
6434	090219	2008	BO	66 07.8 N	027 18.7 W	520	5	8	CTD,LADCP,Chemistry
6434	090219	2024	EN	66 07.7 N	027 19.4 W	520	5	8	CTD,LADCP,Chemistry
6435	090219	2103	BE	66 11.0 N	027 31.6 W	486	5	10	CTD,LADCP,Chemistry
6435	090219	2116	BO	66 11.0 N	027 32.0 W	486	5	10	CTD,LADCP,Chemistry
6435	090219	2132	EN	66 11.0 N	027 32.3 W	486	5	10	CTD,LADCP,Chemistry
6436	090219	2216	BE	66 14.8 N	027 45.2 W	478	4	12	CTD,LADCP,Chemistry
6436	090219	2231	BO	66 14.9 N	027 45.3 W	478	4	12	CTD,LADCP,Chemistry
6436	090219	2256	EN	66 15.0 N	027 45.5 W	478	4	12	CTD,LADCP,Chemistry
6437	090319	0000	BE	66 19.9 N	028 07.9 W	344	6	12	CTD,LADCP,Chemistry
6437	090319	0013	BO	66 20.1 N	028 08.1 W	344	6	12	CTD,LADCP,Chemistry
6437	090319	0036	EN	66 20.3 N	028 07.6 W	344	6	12	CTD,LADCP,Chemistry
6438	090319	0146	BE	66 14.9 N	027 45.6 W	470	4	11	CTD,LADCP,Chemistry
6438	090319	0202	BO	66 14.8 N	027 45.3 W	470	4	11	CTD,LADCP,Chemistry
6438	090319	0227	EN	66 14.7 N	027 45.3 W	470	4	11	CTD,LADCP,Chemistry
6439	090319	0310	BE	66 11.2 N	027 31.6 W	484	5	10	CTD,LADCP,Chemistry
6439	090319	0326	BO	66 10.9 N	027 31.6 W	484	5	10	CTD,LADCP,Chemistry
6439	090319	0347	EN	66 10.6 N	027 32.0 W	484	5	10	CTD,LADCP,Chemistry
6440	090319	0433	BE	66 07.9 N	027 18.8 W	517	2	11	CTD,LADCP,Chemistry
6440	090319	0448	BO	66 07.8 N	027 19.0 W	517	2	11	CTD,LADCP,Chemistry
6440	090319	0516	EN	66 07.2 N	027 19.8 W	517	2	11	CTD,LADCP,Chemistry

6441	090319	0548	BE	66 06.4 N	027 11.9 W	617	7		CTD,LADCP
6441	090319	0605	BO	66 06.1 N	027 12.4 W	617	7		CTD,LADCP
6441	090319	0617	EN	66 05.8 N	027 12.9 W	617	7		CTD,LADCP
6442	090319	0643	BE	66 05.0 N	027 05.4 W	655	5	13	CTD,LADCP,Chemistry
6442	090319	0702	BO	66 04.8 N	027 05.3 W	655	5	13	CTD,LADCP,Chemistry
6442	090319	0723	EN	66 04.6 N	027 05.7 W	655	5	13	CTD,LADCP,Chemistry
6443	090319	0753	BE	66 02.7 N	026 57.2 W	595	5		CTD,LADCP
6443	090319	0809	BO	66 02.8 N	026 56.9 W	595	5		CTD,LADCP
6443	090319	0822	EN	66 02.9 N	026 56.7 W	595	5		CTD,LADCP
6444	090319	0849	BE	66 00.8 N	026 49.1 W	455	4	9	CTD,LADCP,Chemistry
6444	090319	0904	BO	66 00.9 N	026 48.3 W	455	4	9	CTD,LADCP,Chemistry
6444	090319	0919	EN	66 01.3 N	026 48.0 W	455	4	9	CTD,LADCP,Chemistry
6445	090319	1025	BE	65 56.0 N	026 29.5 W	292	5	10	CTD,LADCP,Chemistry
6445	090319	1037	BO	65 56.1 N	026 28.9 W	292	5	10	CTD,LADCP,Chemistry
6445	090319	1051	EN	65 56.4 N	026 28.9 W	292	5	10	CTD,LADCP,Chemistry

Table 2

Sta.	Date	UTC	Latitude	Longitude	Depth, m	Geological sampling
6320	22.08.2019	13:50	59 ° 29.788 N	29 ° 21.126 W	1413	Grab, MC
6446	04.09.2019	6:58	66 ° 44.954 N	18 ° 47.880 W	694	Grab, MC, GC

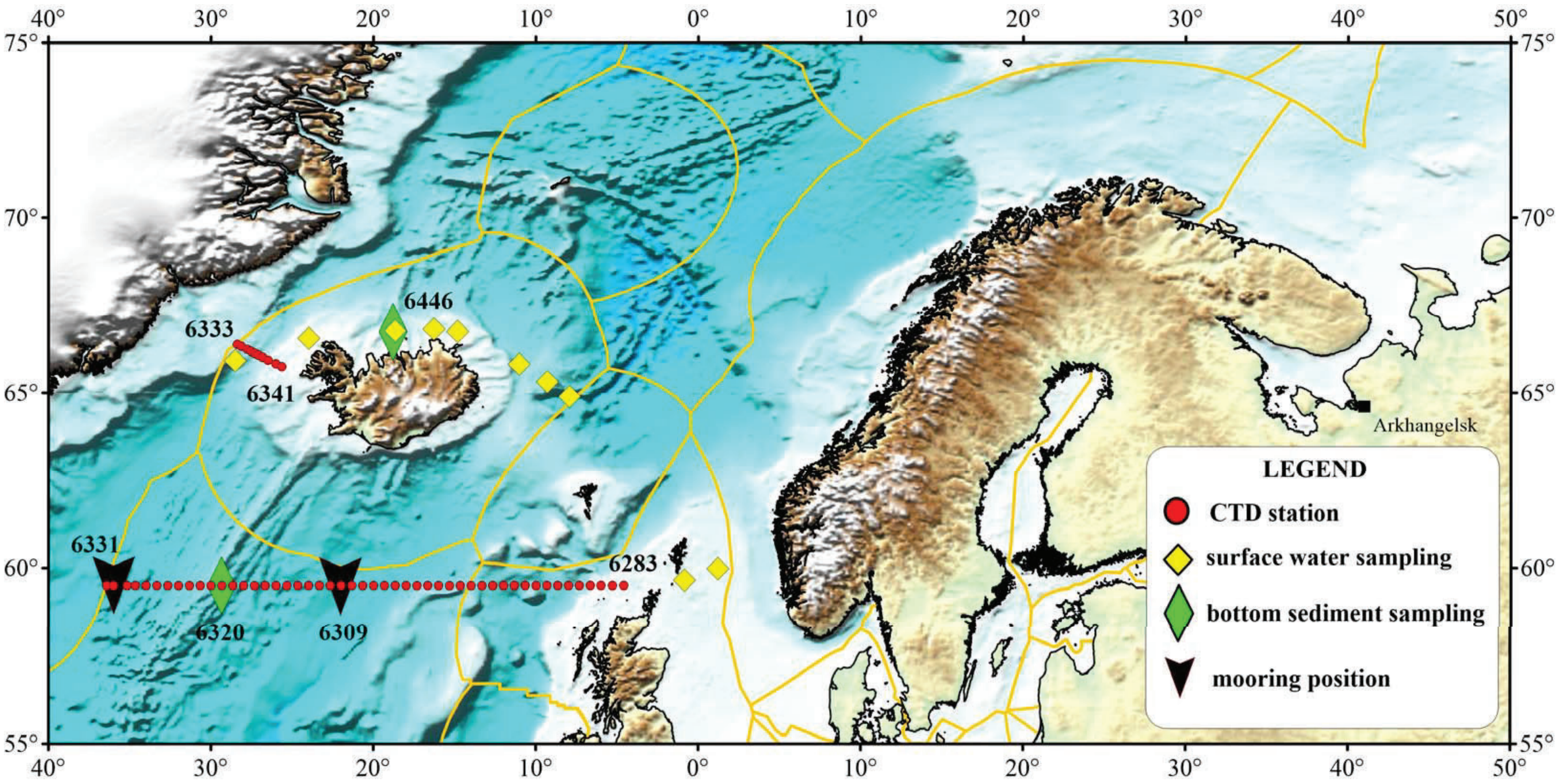

Fig. 1 Station locations with legend.

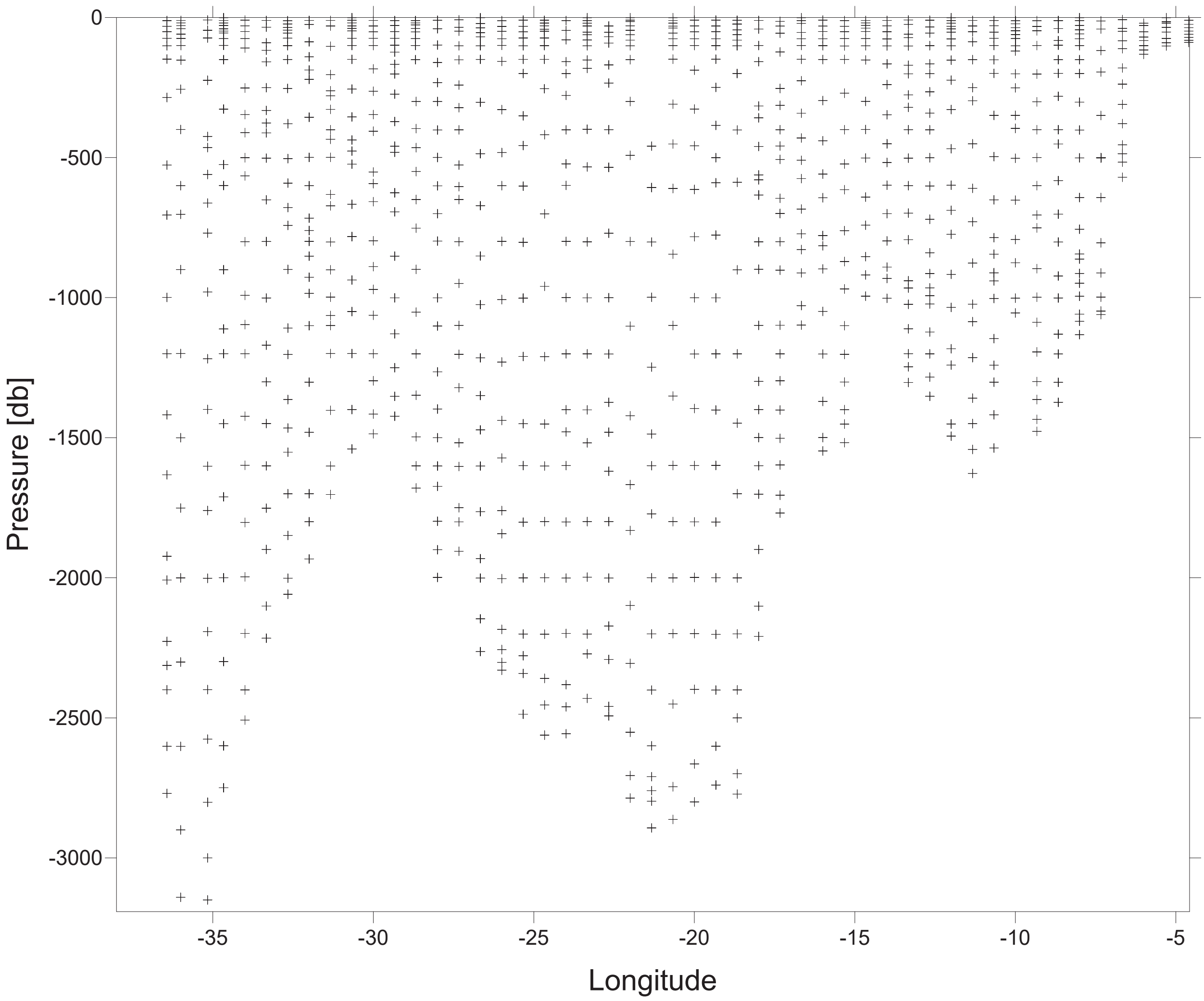

Figure 2. Vertical distribution of samples along the 59.5 section.

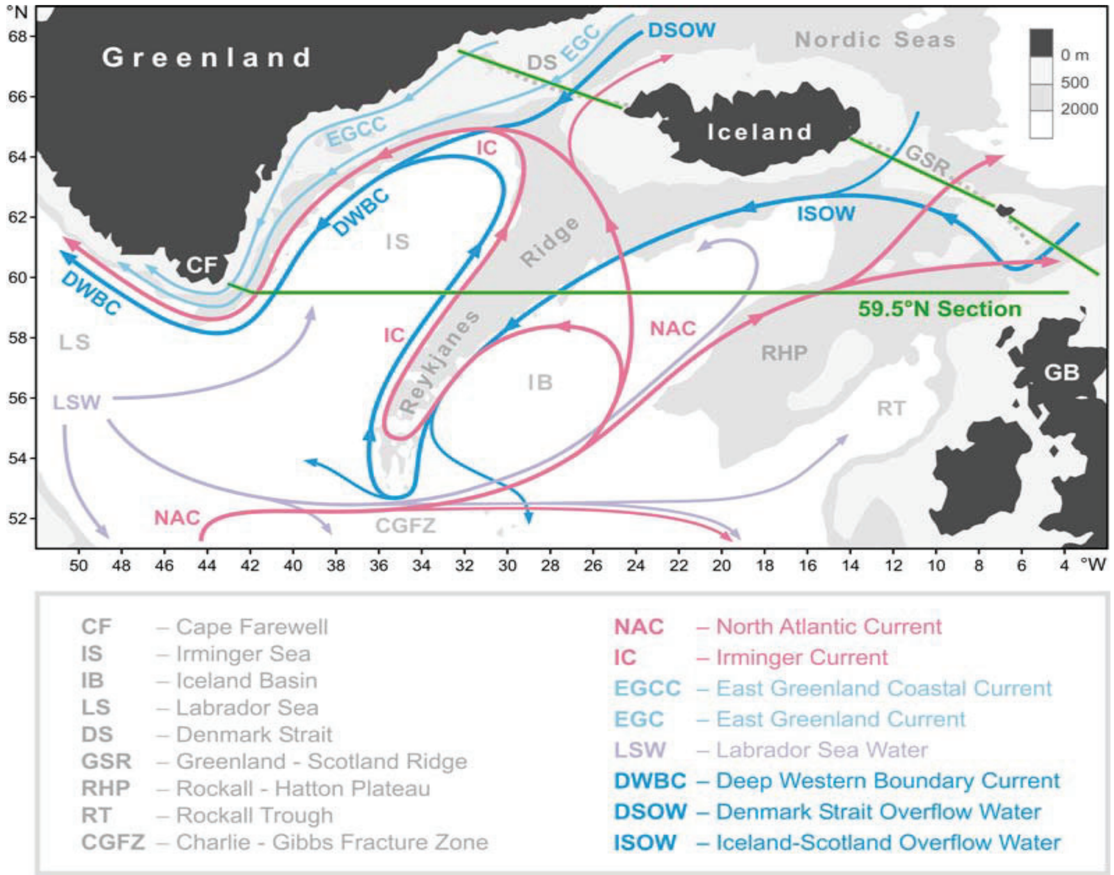

Figure 3. Schematic diagram of the large-scale circulation in the northern North Atlantic compiled from [Schmitz and McCartney, 1993; Schott and Brandt, 2007; Sutherland and Pickart, 2008; Lherminier et al., 2010]. Abbreviations for the main topographic features, currents and water masses are explained in the legend. The nominal locations of the 59.5°N hydrographic section (1997 – present) and sections across the straits between Greenland, Iceland, Faeroe and Shetland Islands (2011 – present) are shown with the solid green lines.

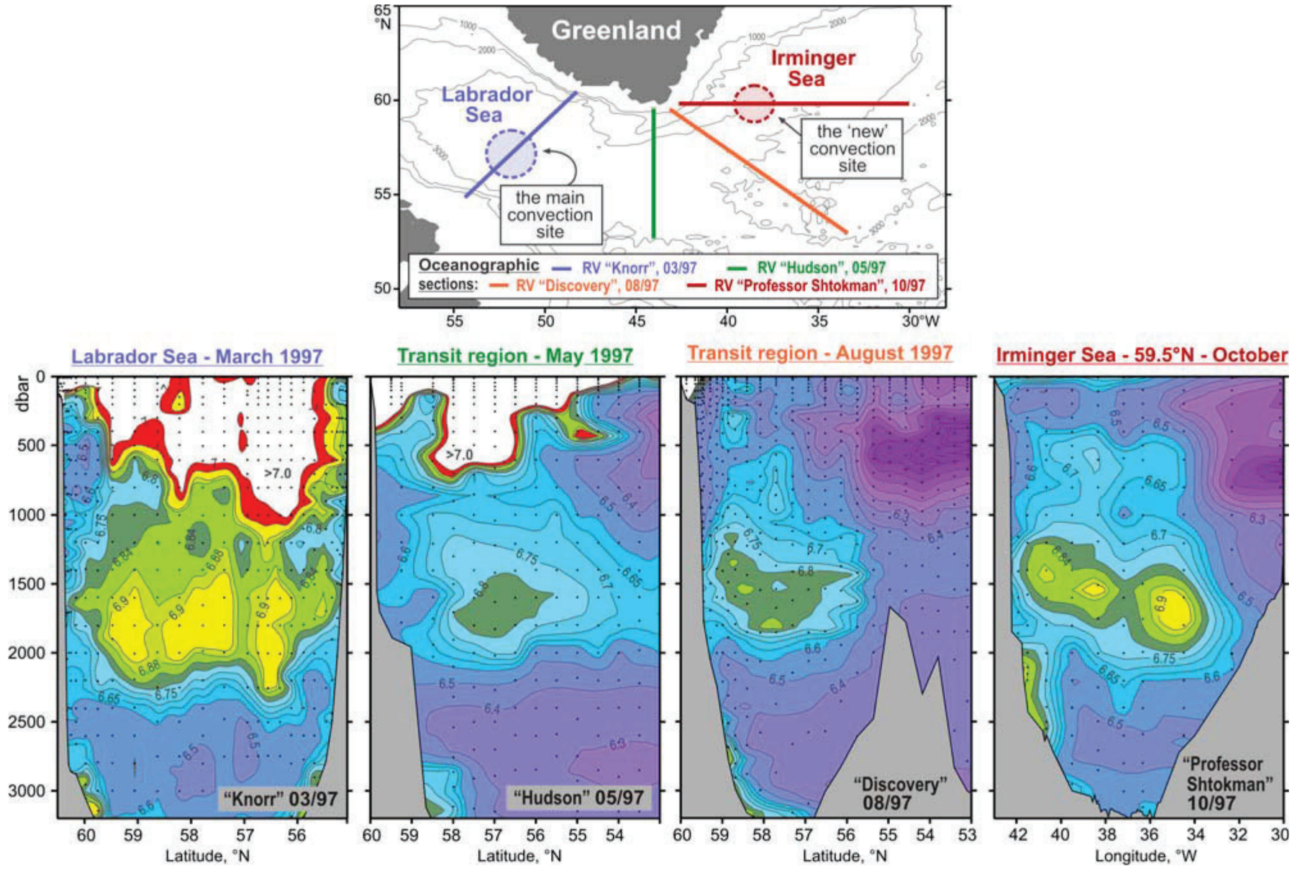

Figure 4. Oxygen concentrations (ml/l) in the water column (lower panel) as observed in March–October 1997 in four hydrographic sections (upper panel) ending nearby the southern tip of Greenland. A separate oxygen maximum in the LSW layer (1000–2000 m) in the Irminger Sea at 59.5°N strongly implies local convective renewal of LSW before 1997. Adapted from [Falina et al., 2007].

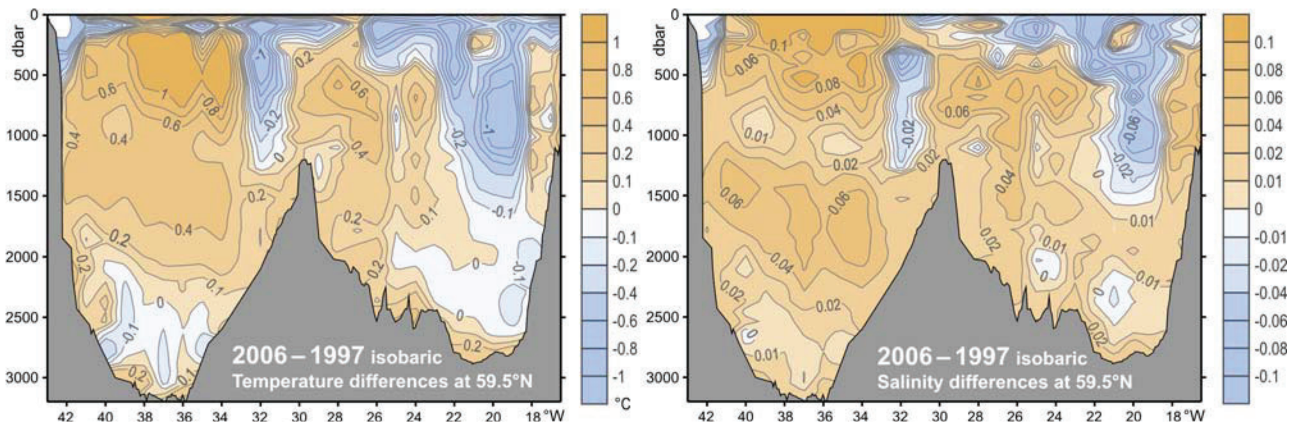

Figure 5. Warming and salinification in the northern North Atlantic between the mid-1990s and mid-2000s, as observed at 59.5°N. The figure shows the 2006–1997 temperature (°C, left) and salinity (right) differences on isobaric surfaces in the Irminger Sea and Iceland Basin. Adapted from [Sarafanov et al., 2007].

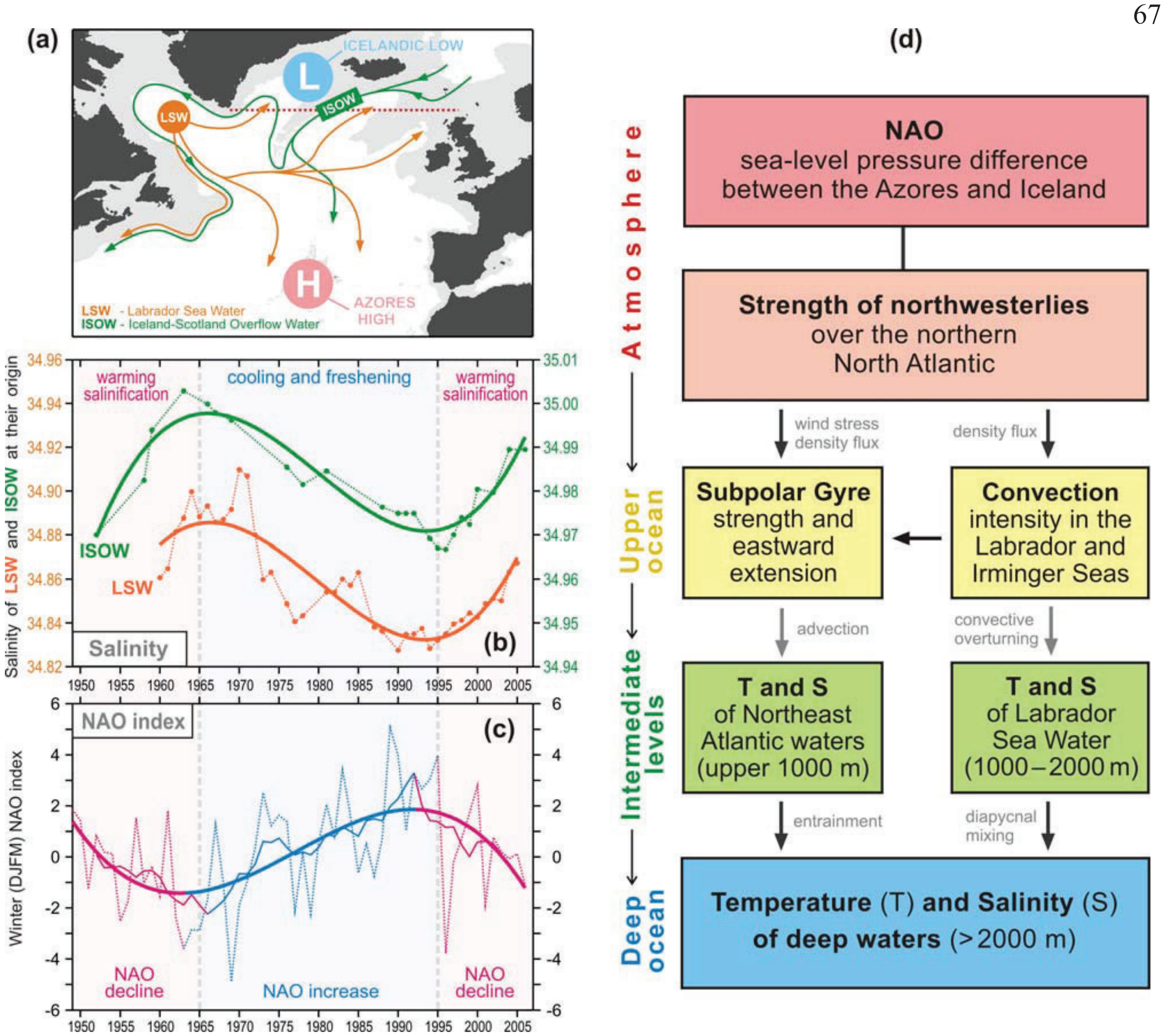

Figure 6. Coherence of the decadal salinity changes (1950s – 2000s) of the intermediate (LSW) and deep (ISOW) waters in the northern North Atlantic and their link to the North Atlantic Oscillation (NAO) index. **(a)** Schematic representation of the LSW and ISOW pathways and locations of the Icelandic Low (L) and Azores High (H) centers constituting the NAO dipole pattern. The red dotted line indicates the 59.5°N transatlantic section. **(b)** Salinity time series for LSW in the Labrador Sea [Yashayaev, 2007] and ISOW in the Iceland basin [Boessenkool et al., 2007; Sarafanov et al., 2007] overlaid by the third order polynomial fits. **(c)** Time series of the winter NAO index, after [Hurrell, 1995], overlaid by 7-year running mean and third order polynomial fit. **(d)** Mechanism of the NAO effect on the decadal changes in temperature (T) and salinity (S) of the northern North Atlantic intermediate and deep waters. Positive / negative links shown with the dark / light grey arrows mean that changes in 'causative' and 'consequential' characteristics have the same / opposite sign(s). The overall effect of the NAO on T and S of the in the water column is negative: persistent NAO decline leads to warming and salinification of the water masses and vice versa, as shown in (b) and (c). Adapted from [Sarafanov, 2009].

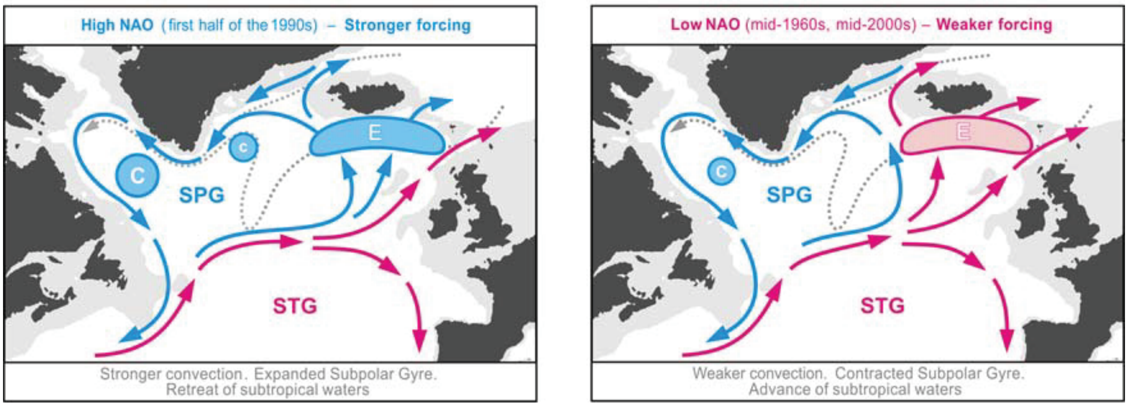

Figure 7. Schematic representation of the upper-ocean circulation and convection intensity in the northern North Atlantic under high (left) and low (right) NAO conditions. Blue (magenta) solid arrows indicate the upper-ocean flows with higher fraction of colder fresher subpolar (warmer saltier subtropical) waters. The main pathways of the Nordic overflow-derived deep waters are shown with the dotted curves. "C" and "E" symbols are used to denote, respectively, the deep convection sites and the domain, where the Atlantic waters are entrained into ISOW. Larger (smaller) circles indicate stronger (weaker) convection. SPG and STG – the subpolar and subtropical gyres, respectively. Adapted from [Sarafanov, 2009].

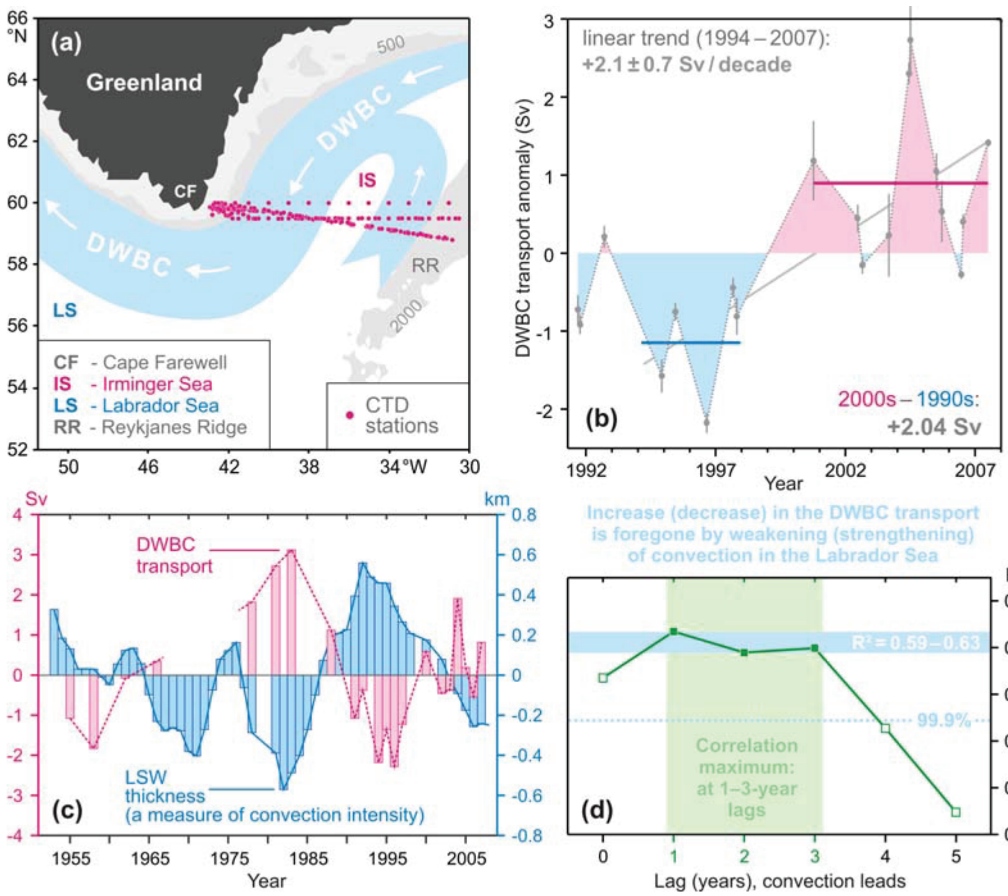

Figure 8. The Deep Western Boundary Current (DWBC) transport variability and its link to the convection intensity in the Labrador Sea. **(a)** Locations of the hydrographic sections (1991–2007) and schematic of the deep water circulation in the Irminger Sea. **(b)** The DWBC transport anomalies at Cape Farewell in 1991–2007, $1\ Sv = 10^6\ m^3\ s^{-1}$. The 1994–1997 and 2000–2007 mean anomalies and the 1994–2007 linear trend are shown. **(c)** Anomalies of the DWBC transport at Cape Farewell and the Labrador Sea Water (LSW) thickness in the Labrador Sea in the 1950s–2000s. **(d)** Correlation coefficient (R^2) for the two times series shown in **(c)** at the 0–5-year lag, the LSW thickness leads. The correlation maximum is achieved at the 1–3-year lag. The DWBC transport anomalies in the southern Irminger Sea are foregone by the convection intensity anomalies in the Labrador Sea. Adapted from [Sarafanov et al., 2009].

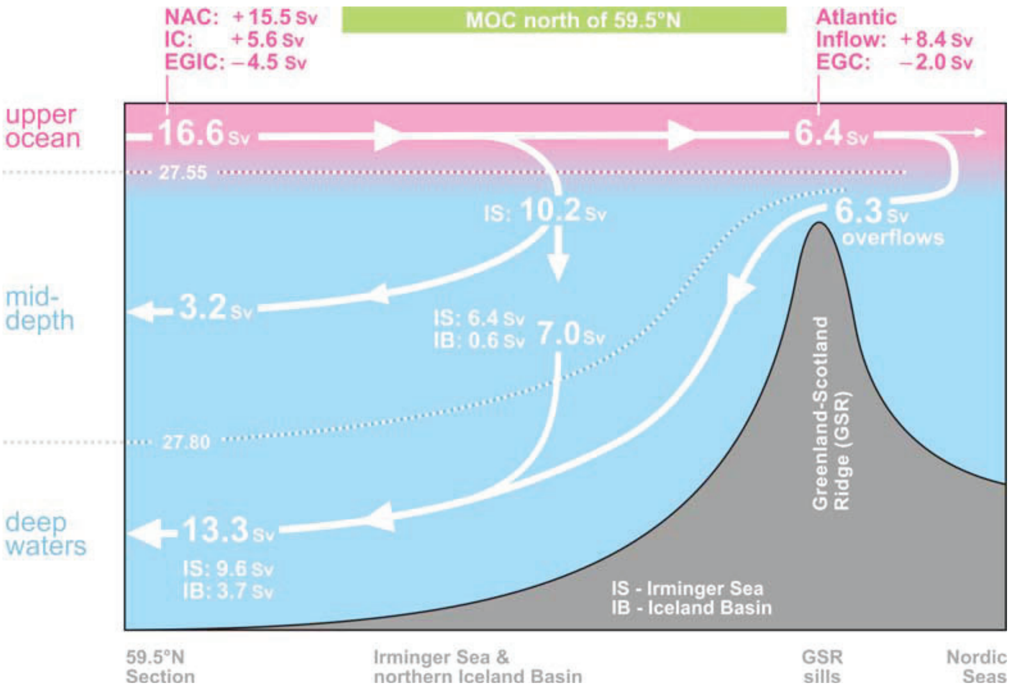

Figure 9. Schematic diagram of the Meridional Overturning Circulation (MOC) at the northern periphery of the Atlantic Ocean, northeast of Cape Farewell. The dotted lines refer to the σ_0 isopycnals 27.55 and 27.80. The arrows denote the integral meridional and diapycnal volume fluxes. Where the signs are specified, the positive (negative) transports are northward (southward). The NAC and EGIC transports in the upper layer ($\sigma_0 < 27.55$) at 59.5°N are the throughputs accounting for the recirculations. EGIC – the East Greenland / Irminger Current – refers to the upper part of the Western Boundary Current. Other abbreviations are explained in the legend to **Figure 3**. Adapted from [Sarafanov et al., 2012].

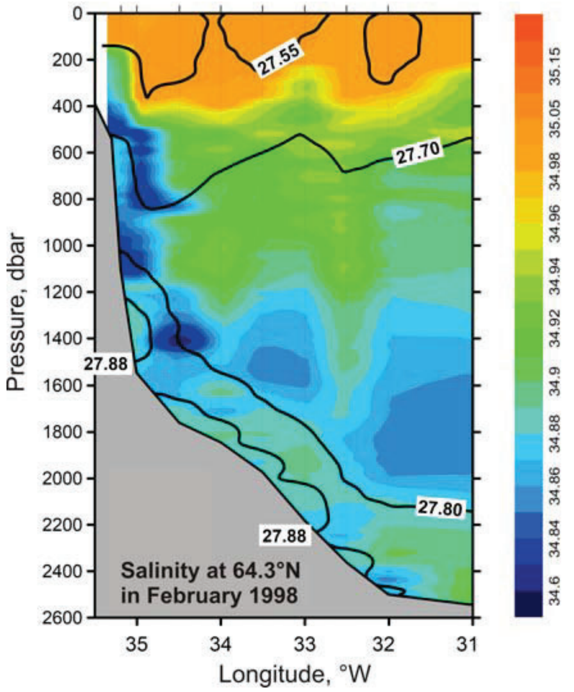

Figure 10. Salinity observed in the northwestern Irminger Sea at 64.3°N in February 1998. The σ_0 isopycnals 27.55, 27.70, 27.80 and 27.88 are plotted as the thick black lines; the station locations are marked with the ticks on the top axis. The plot shows fresh dense waters descending (cascading) down the continental slope of Greenland down to the LSW layer ($27.70 < \sigma_0 < 27.80$) and the layer of the Nordic Seas overflow-derived deep waters ($\sigma_0 > 27.80$). Adapted from [Falina et al., 2012].

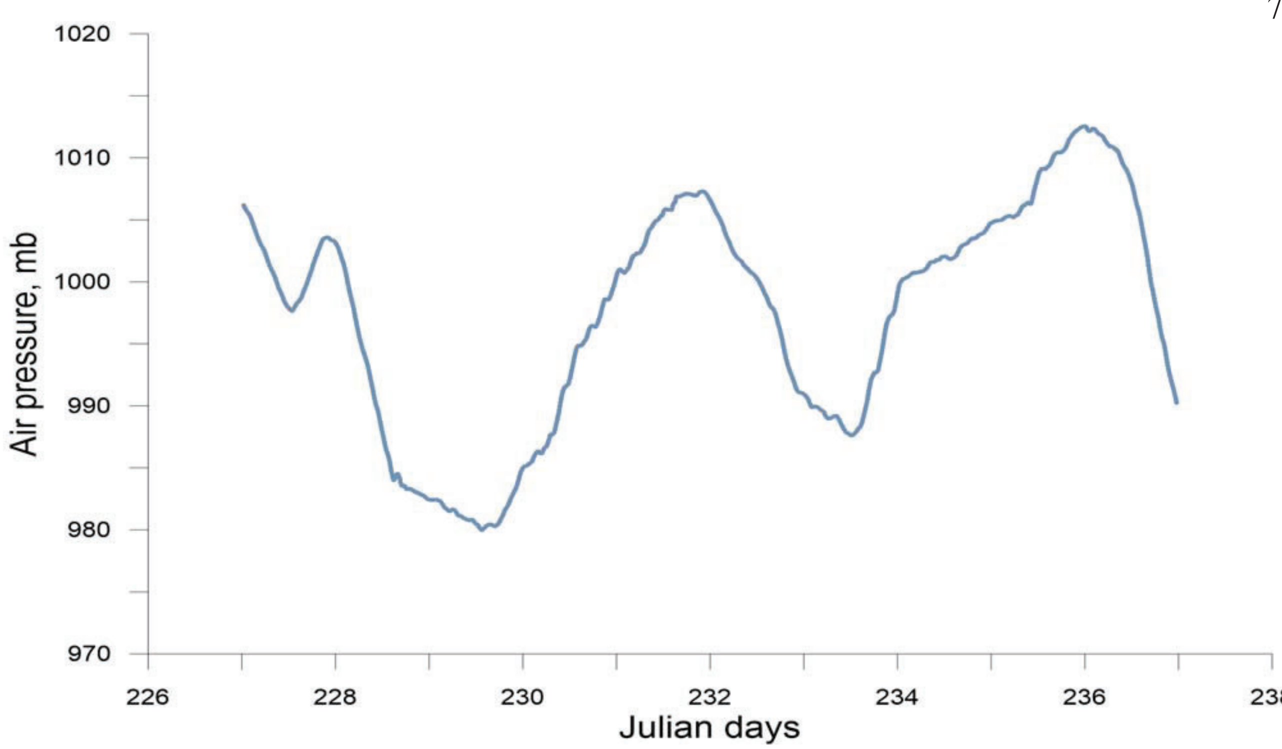

Figure 11. One-hour averaged atmospheric pressure (mb) measured during the 59.5 section 77 cruise of *Akademik Mstislav Keldysh*.

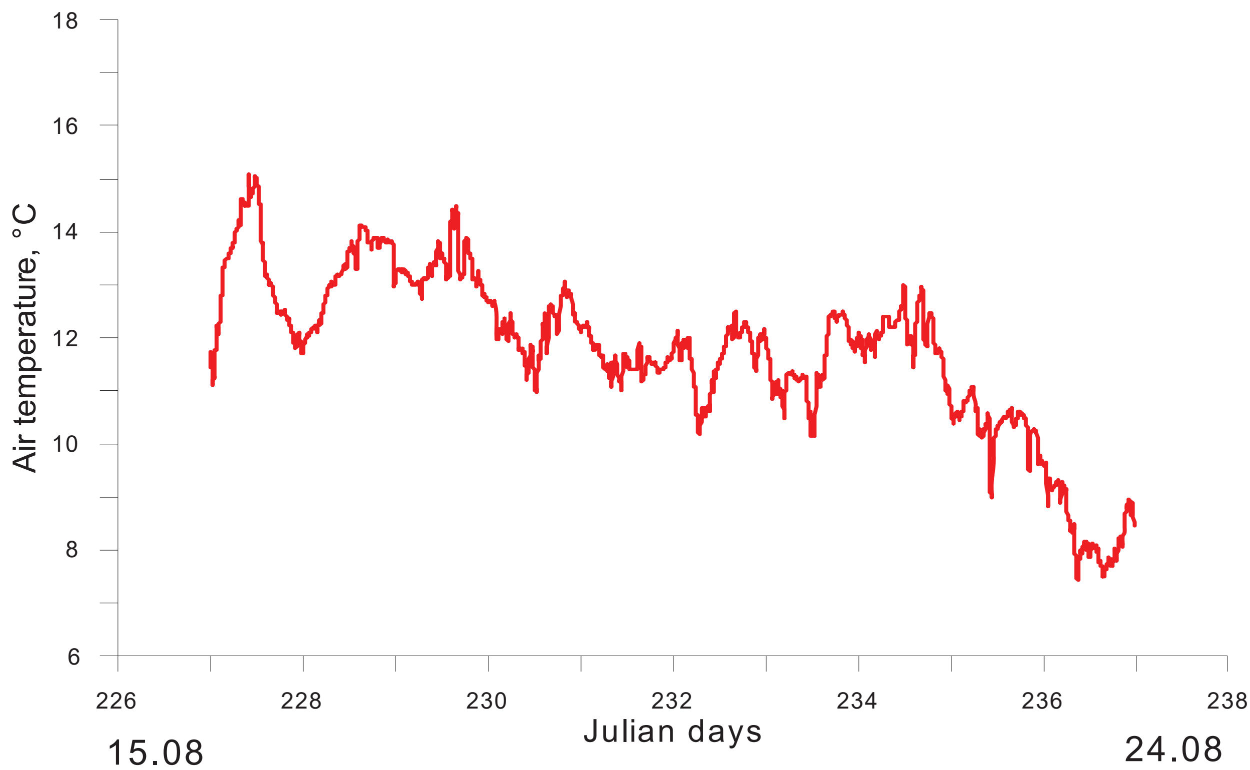

Figure 12. One-hour air temperature (°C) measured during the 59.5 section 77 cruise of *Akademik Mstislav Keldysh*.

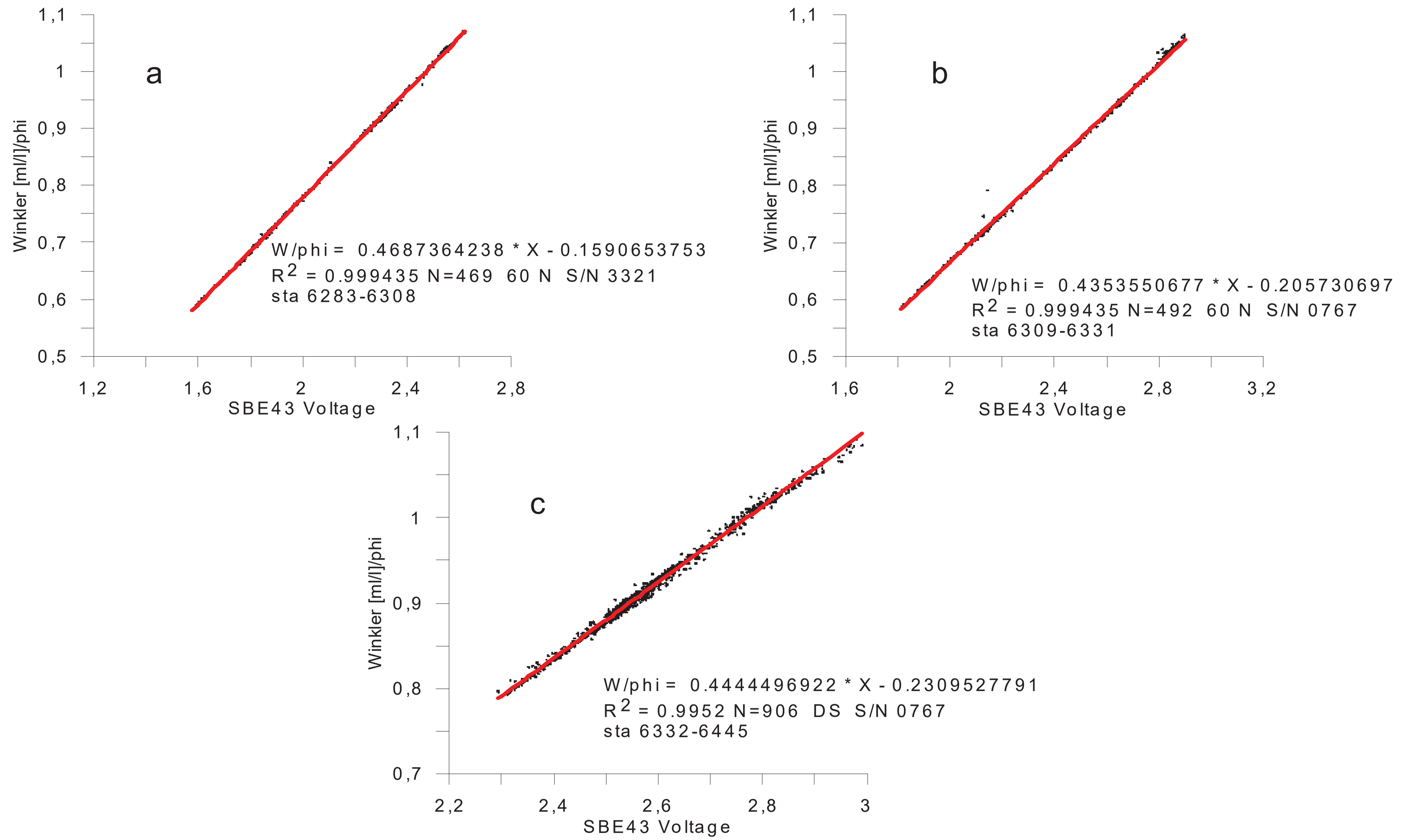

Figure 13 Regression lines for Winkler oxygen divided by φ versus SBE 43 output voltage for (a) 59.5 transatlantic section (SN 3321), (b) 59.5 transatlantic section (SN 0699), (c) the DS experiment II.

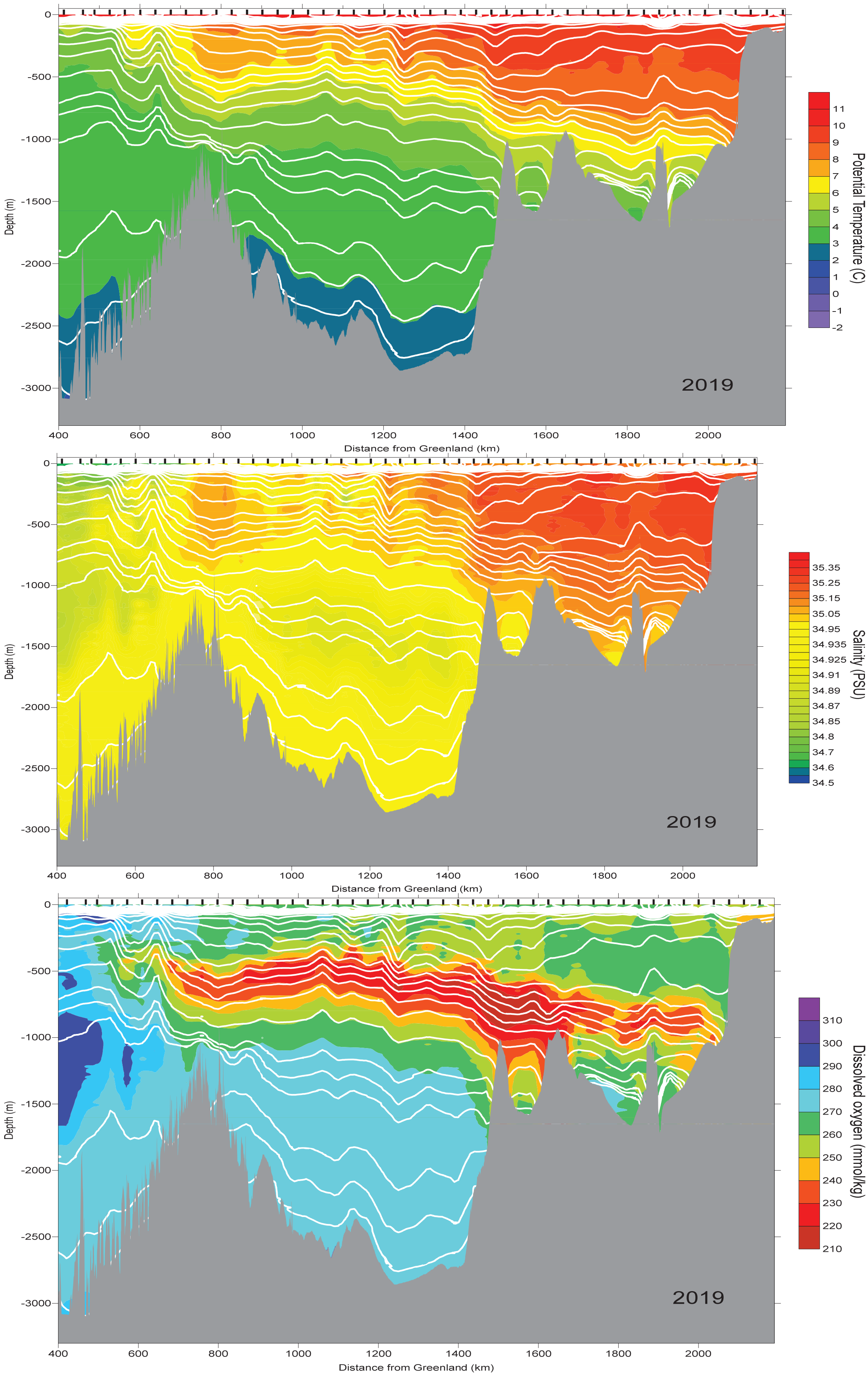

Figure 14 The vertical distribution of (a) potential temperature (°C) and (b) salinity (PSU) (c) dissolved oxygen (μmol/kg) along 59.5 N in 15 -24 August 2019. Potential density is shown in white. Station position is shown by vertical marks.